Exact ground-state correlation functions of the one-dimensional Emery model in the strong-coupling limit

P.-A. Bares* and P. A. Lee
Department of Physics, Massachusetts Institute of Technology, Cambridge, Massachusetts 02139
(Received 16 September 1993)

We investigate a recently constructed ground state of the one-dimensional Emery model in the infinite-U limit with two holes per unit cell and a restricted range of parameters. We show that the ground state is unique and evaluate exactly the equal-time correlation functions which we find to decay exponentially with distance. In a certain range of parameters, the model incorporates the physics of the Kondo insulator. Our exact results imply the absence of off-diagonal long-range order or power-law correlation for singlet pairing. The ground state of the doped Emery chain exhibits a massive degeneracy. The additional charges are found to be exponentially localized around the insertion sites.

I. INTRODUCTION

Recently, Brandt and Giesekus[1] constructed the exact ground states of the Hubbard model with infinite on-site repulsion on ($D \geq 2$)-dimensional perovskitelike lattices as well as of the periodic Anderson model for a certain range of parameters. In Refs. 2–4, the method was extended to the one-dimensional (1D) periodic Anderson model, to the 1D Emery model, to a modified d-p model in two dimensions, and to a Hubbard model with nearest-neighbor and bond-charge interactions. These solutions are subject to restrictions on the parameters of the theory and involve an even number of (spin-1/2) electrons per unit cell.[5] The ground-state wave functions have a local character and correspond to a fermionic realization of the valence bond solid (VBS) ground states occurring in certain isotropic quantum antiferromagnets.[6] In the latter case, it has been shown rigorously that the spin Hamiltonian has a unique ground state, a gap in the excitation spectrum, and exponentially decaying ground-state correlation functions. In contrast, little is known about the physical properties of the fermionic ground states introduced in Refs. 1–4. For instance, in various cases it is not known whether the ground state is unique (see the discussions in Refs. 1–3), and there is even speculation that it is superconducting.[7]

In this paper we provide technical details for the derivation of the results in Ref. 8. Below, we show that the ground state is unique[9] and evaluate exactly the equal-time ground-state correlation functions of the 1D Emery model when the on-site repulsion on the Cu sites is infinite. The extension of our approach to the periodic Anderson model and other Kondo lattices is possible in one dimension, even though the latter models involve larger matrices than we have to handle in this work.[8] For the Emery model, which is the simplest among this class of models, we find exponential decay in the singlet pairing channel and in all correlation functions. We argue that this type of wave function describes an insulator, and in a certain range of parameters, incorporates the physics of Kondo insulators.

Consider the 1D Emery model in the strong-coupling limit, i.e.,

$$H_{\mathcal{E}} = \mathcal{P}\Big\{ t \sum_{i,\sigma} \left[p^{\dagger}_{i+1\sigma} p_{i,\sigma} + \text{H.c.} \right] + \epsilon_p \sum_{i,\sigma} p^{\dagger}_{i,\sigma} p_{i,\sigma} + \epsilon_d \sum_{i,\sigma} d^{\dagger}_{i,\sigma} d_{i,\sigma} + V \sum_{i,\sigma} \times \left[d^{\dagger}_{i,\sigma} \left(p_{i+1\sigma} - p_{i,\sigma} \right) + \text{H.c.} \right] \Big\} \mathcal{P} , \tag{1}$$

where the subscript i runs over L unit cells consisting of one O site and one Cu site (see Fig. 1). We employ the hole picture where $d^{\dagger}_{i\sigma}$ creates a hole of spin σ at a Cu site. The energy of a single hole ($3d^9$ configuration) is ϵ_d and that of two holes is infinite. The operator $\mathcal{P}$ projects out the two-hole configurations. We restrict our discussion to the spin $s = 1/2$ case and note that the generalization to higher spin and/or degeneracy is straightforward.[8]

In Ref. 3, an exact ground state of the model (1) for two particles (spin $s = \frac{1}{2}$) per unit cell has been constructed as[5]

$$|\Psi_0\rangle = \mathcal{P} \prod_{i=1,\sigma}^{L} \alpha^{\dagger}_{i,\sigma} |0\rangle , \tag{2}$$

where

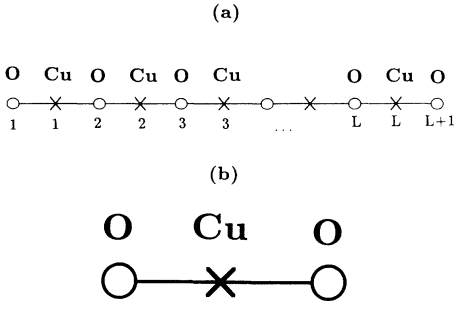

FIG. 1. (a) The unit cell comprises one O and one Cu ion. The labeling of the sites is that of the unit cells. (b) A cluster consists of one central Cu ion and two adjacent O ions.

$$\alpha^{\dagger}_{i,\sigma} = \frac{1}{\sqrt{1+2\widetilde{V}^{-2}}}\left(d^{\dagger}_{i,\sigma} - \widetilde{V}^{-1}\left[p^{\dagger}_{i+1,\sigma} - p^{\dagger}_{i,\sigma}\right]\right) , \quad (3)$$

and $\widetilde{V} = \frac{V}{t}$ denotes a dimensionless interaction parameter. The wave function (2) is an eigenstate of the Hamiltonian (1) with open boundary conditions (OBC) provided the parameters of the model are restricted to the manifold

$$\epsilon_d - \epsilon_p = 2t\left(1-\widetilde{V}^2\right) . \quad (4)$$

To get some insight into the physical problems described by the restricted parameter space, consider the limits $\widetilde{V} \to \infty$ and $\widetilde{V} \to 0$. For $\widetilde{V} \gg 1$, $\epsilon_d - \epsilon_p \ll -2t$ so that the d level should be nearly fully occupied. This corresponds to the Kondo lattice regime with one Kondo site and one conduction electron per unit cell. Futhermore, the effective exchange $J \approx \frac{V^2}{\epsilon_p - \epsilon_d}$ is comparable to the direct hopping t between conduction holes; therefore we are in the intermediate-coupling limit for the Kondo lattice. In the opposite limit $\widetilde{V} \ll 1$, $\epsilon_d - \epsilon_p \approx 2t$, i.e., the d level crosses near the top of the conduction band and the occupation of the Cu site should be small. On physical grounds, we expect the constraint of no double occupancy to be ineffective in this limit, i.e., the system can be described by hybridized p and d bands. A simple calculation leads to a dispersionless upper band located at $\epsilon_p + 2t$ and a lower band given by $\epsilon_-(k) = \epsilon_p - \frac{V^2}{t} + 2t\cos(k)$, resulting in an insulator with a gap $\frac{V^2}{t}$. We shall verify that this is indeed consistent with our exact results.

The plan of the paper is as follows: In Sec. II, we present a proof of the uniqueness of the ground state. Some details of the proof are deferred to Appendix A. Section III is devoted to the evaluation of the ground-state correlation functions. Appendix B contains the explicit form of some matrices and right (left) eigenvectors used in Sec. III. In Sec. IV we deal with doping effects and discuss various extensions of previous work. Section VI contains the concluding remarks.

II. UNIQUENESS OF THE GROUND STATE

In this section we prove the uniqueness of the ground state of the 1D Emery model $H_{\mathcal{E}}$.[8] Following Refs. 1–3, it is convenient to rewrite the Hamiltonian (1) for a system with L unit cells as

$$H_{\mathcal{E}} = \mathcal{P}\left[-N_\sigma C + (\epsilon_p + 2t)\widehat{n}\right]\mathcal{P}L + H_> , \quad (5)$$

where $N_\sigma = 2$ (for spin $s = 1/2$) is the degeneracy, $C = 2t + \frac{V^2}{t}$, $\widehat{n} = \frac{1}{L}\sum_{i\sigma}\left(d^{\dagger}_{i\sigma}d_{i\sigma} + p^{\dagger}_{i,\sigma}p_{i,\sigma}\right)$, and $H_> = C\sum_{i,\sigma}\widetilde{\alpha}_{i,\sigma}\widetilde{\alpha}^{\dagger}_{i,\sigma}$ denotes a positive semidefinite piece, with $\widetilde{\alpha}^{\dagger}_{i,\sigma} = \mathcal{P}\alpha^{\dagger}_{i,\sigma}\mathcal{P}$. When acting on the state (2), the first term on the right-hand side of (5) gives a c number while the second term vanishes by virtue of the property $\left[\widetilde{\alpha}^{\dagger}_{i,\sigma}\right]^2 = 0$. Therefore (2) is a ground state of (1). However, from the above argument it is not clear that the ground state is nondegenerate. Since $H_>$ is positive semidefinite, the ground state of the system must fulfill $\langle\Psi_0|H_>|\Psi_0\rangle = 0$, ergo $\sum_{i,\sigma}\|\widetilde{\alpha}^{\dagger}_{i,\sigma}|\Psi_0\rangle\|^2 = 0$ which in turn implies that

$$\widetilde{\alpha}^{\dagger}_{i,\sigma}|\Psi_0\rangle = 0 , \quad (6)$$

for $i = 1,\ldots,L$ and $\sigma = \uparrow,\downarrow$. The set of equations (6) impose very strong constraints on the state $|\Psi_0\rangle$. In Appendix A, we show, by expanding $|\Psi_0\rangle$ into a complete set of states and by eliminating the configurations that are inconsistent with the set of Eq. (6), that the ground state should be of the form

$$|\Psi_0\rangle = \sum_{\{\nu\}}\sum_{\{\nu'\}} A(\nu_1,\ldots,\nu_L|\nu'_1,\ldots,\nu'_L)c^{\dagger}_{\nu_1\uparrow}\ldots c^{\dagger}_{\nu_L\uparrow}c^{\dagger}_{\nu'_1\downarrow}\ldots c^{\dagger}_{\nu'_L\downarrow}|0\rangle , \quad (7)$$

where $\{\nu\} = \{\nu_1 \le \nu_2 \le \cdots \le \nu_L\}$ and the summation index ν_j runs over all sites assigned to the jth cluster (a cluster involves three sites, one Cu site and two adjacent O sites, see Fig. 1). For generality's sake, we write the cluster operators as $\widetilde{\alpha}^{\dagger}_{i\sigma} = \sum_{\mu_i} a_{\mu_i}c^{\dagger}_{\mu_i\sigma}$, where the coefficients a_{μ_i} are independent of the spin label [see Eq. (3)] and $c^{\dagger}_{\nu_i\sigma}$ denotes a fermion *or* a Hubbard operator with the property that $\left[c^{\dagger}_{\mu_i\sigma}\right]^2 = 0$. The amplitudes $A(\ldots)$ are not assumed to be antisymmetric and the constraint of no double occupancy is automatically taken into account in the commutation rules of the Hubbard operators, i.e., $A(\nu_1,\ldots,\nu_L|\nu'_1,\ldots,\nu'_L)$ need not vanish when ν_j, referring to a Cu site, coincides with ν'_j.

Let us rewrite explicitly the equations (6), say, for the up-spin cluster operator,

$$\sum_{\{\nu'\}}\sum_{\{\nu\}}\sum_{\mu_j} a_{\mu_j}A(\nu_1,\ldots,\nu_L|\nu'_1,\ldots,\nu'_L)c^{\dagger}_{\mu_j\uparrow}c^{\dagger}_{\nu_1\uparrow}\ldots c^{\dagger}_{\nu_L\uparrow}c^{\dagger}_{\nu'_1\downarrow}\ldots c^{\dagger}_{\nu'_L\downarrow}|0\rangle = 0 , \quad (8)$$

for $j = 1,\ldots,L$. In the expansion (8), the components for which μ_j coincides with one of the ν_j vanish as $\left[c^{\dagger}_{\nu_j\uparrow}\right]^2 = 0$. Moreover, if $c^{\dagger}_{\nu_j}$ is a Hubbard operator, there is no contribution from the term where $\mu_j = \nu'_j$. The remaining nonvanishing terms contain configurations whose coefficients appear in pairs, since in (7) only one up spin and one down spin are assigned to each cluster. For example, we have terms such as

$$a_{\mu_j}A(\nu_1,\ldots,\nu_j,\ldots,\nu_L|\nu'_1,\ldots,\nu'_L)c^{\dagger}_{\mu_j\uparrow}c^{\dagger}_{\nu_1\uparrow}\ldots c^{\dagger}_{\nu_j\uparrow}\ldots c^{\dagger}_{\nu_L\uparrow}c^{\dagger}_{\nu'_1\downarrow}\ldots c^{\dagger}_{\nu'_L\downarrow}|0\rangle , \quad (9)$$

and

$$a_{\nu_j} A(\nu_1,\ldots,\mu_j,\ldots,\nu_L|\nu'_1,\ldots,\nu'_L) c^\dagger_{\nu_j\uparrow} c^\dagger_{\nu_1\uparrow}\cdots c^\dagger_{\mu_j\uparrow}\cdots c^\dagger_{\nu_L\uparrow} c^\dagger_{\nu'_1\downarrow}\cdots c^\dagger_{\nu_L\downarrow}|0\rangle \ . \tag{10}$$

Interchanging the order of the $c^\dagger$'s in (9) and (10), and grouping the coefficients multiplying identical configurations, we infer that the amplitudes should fullfill

$$\frac{a_{\mu_j}}{a_{\nu_j}} = \frac{A(\nu_1,\ldots,\mu_j,\ldots,\nu_L|\nu'_1,\ldots,\nu'_L)}{A(\nu_1,\ldots,\nu_j,\ldots,\nu_L|\nu'_1,\ldots,\nu'_L)} \ , \tag{11}$$

for all appropriate μ_j and ν_j, with $j = 1,\ldots,L$. Similarly, we obtain a set of equations for the down spins as

$$\frac{a_{\mu'_j}}{a_{\nu'_j}} = \frac{A(\nu_1,\ldots,\nu_L|\nu'_1,\ldots,\mu'_j,\ldots,\nu'_L)}{A(\nu_1,\ldots,\nu_L|\nu'_1,\ldots,\nu'_j,\ldots,\nu'_L)} \ , \tag{12}$$

for appropriate μ'_j and ν'_j with $j = 1,\ldots,L$. Using the fact that, for fixed j, the right-hand sides of (11) and (12) are independent of $\{\nu_1,\ldots\nu_L,\nu'_1,\ldots,\nu'_L\}$, where the indices referring to the jth cluster are excluded, it can be readily seen that the set of Eqs. (11) and (12) has a unique solution given by

$$A(\nu_1,\ldots,\nu_L|\nu'_1,\ldots,\nu'_L) \propto \prod_i a_{\nu_i} a_{\nu'_i} \ . \tag{13}$$

Substituing (13) into the expansion (7), we note that $|\Psi_0\rangle$ has the product form $|\Psi_0\rangle = \prod_{i\sigma} \tilde{\alpha}^\dagger_{i\sigma}|0\rangle$. From the uniqueness of the ground state and the total azimuthal spin $S^z = 0$, it follows immediately that the ground state is a singlet.

III. GROUND-STATE CORRELATION FUNCTIONS

This section is devoted to the evaluation of the equal-time ground-state correlation functions of the 1D Emery model. The method we present is easily extended to other models for which the ground state has a similar structure such as the periodic Anderson model.[8] For the 1D Emery model, we are able to solve the problem analytically. In general, however, the dimension of the matrices involved becomes very large and it is difficult to give a complete analytic solution. Nonetheless, a combination of the algebraic techniques devised in this paper as well as of numerical diagonalization of large matrices permits a complete determination of ground-state properties.

In order to calculate the correlation functions in the ground state, we need to rewrite (2) in a manageable form. The ground-state wave function has a local structure and in this sense shares some resemblance with the VBS ground states occurring in certain spin quantum antiferromagnets.[6] The local nature of the wave function suggests the use of a transfer matrix method.

For clarity's sake, we first evaluate the norm of the ground state (2) in detail. We represent the local degrees of freedom at each O site by a "supervector" $v^\dagger_j$ with transpose

$$\left[v^\dagger_j\right]^T = \left[1, p^\dagger_{j,\uparrow} p^\dagger_{j,\downarrow}, p^\dagger_{j,\uparrow}, p^\dagger_{j,\downarrow}\right] \ . \tag{14}$$

On each Cu site, we define a supermatrix $D^\dagger_i$ as

$$D^\dagger_i = \begin{bmatrix} 0 & \tilde{V}^{-1} & d^\dagger_{i,\downarrow} & -d^\dagger_{i,\uparrow} \\ \tilde{V}^{-1} & 0 & 0 & 0 \\ d^\dagger_{i,\downarrow} & 0 & 0 & -\tilde{V}^{-1} \\ -d^\dagger_{i,\uparrow} & 0 & \tilde{V}^{-1} & 0 \end{bmatrix} . \tag{15}$$

The set of local supermatrices $D^\dagger_i$ form a superalgebra. With these definitions, the wave function (2) can be written as

$$|\Psi_0\rangle = \left[v^\dagger_1\right]^T D^\dagger_1 v^\dagger_2 \left[v^\dagger_2\right]^T D^\dagger_2 \ldots \left[v^\dagger_L\right]^T D^\dagger_L v^\dagger_{L+1}|0\rangle \ , \tag{16}$$

where $|0\rangle$ denotes the vacuum. Note that in this representation the constraint of no double occupancy is obeyed automatically and in contrast to Eq. (2) the projector $\mathcal{P}$ is not necessary. Moreover, it is natural to introduce a supermatrix $\left(P^\dagger_j\right)_{\alpha\beta} = v^\dagger_{j,\alpha} v^\dagger_{j,\beta}$, i.e.,

$$P^\dagger_j = \begin{bmatrix} 1 & p^\dagger_{j,\uparrow} p^\dagger_{j,\downarrow} & p^\dagger_{j,\uparrow} & p^\dagger_{j,\downarrow} \\ p^\dagger_{j,\uparrow} p^\dagger_{j,\downarrow} & 0 & 0 & 0 \\ p^\dagger_{j,\uparrow} & 0 & 0 & p^\dagger_{j,\uparrow} p^\dagger_{j,\downarrow} \\ p^\dagger_{j,\downarrow} & 0 & -p^\dagger_{j,\uparrow} p^\dagger_{j,\downarrow} & 0 \end{bmatrix} , \tag{17}$$

so that the norm of the ground state becomes

$$\langle\Psi_0|\Psi_0\rangle = \langle 0|\left[v_{L+1}\right]^T D_L P_L \ldots P_2 D_1 v_1 \left[v^\dagger_1\right]^T D^\dagger_1 P^\dagger_2 \ldots P^\dagger_L D^\dagger_L v^\dagger_{L+1}|0\rangle \ . \tag{18}$$

In (18) the supermatrix P (D) is the adjoint (transposed and conjugate) of $P^\dagger$ ($D^\dagger$). The expression (18) involves products of (disentangled) site operators while (2) is written in terms of (overlapping) cluster operators. Hence, to calculate the norm of the ground state it is sufficient to evaluate operators in the local site vacua and the problem reduces to a sum of products of c numbers. Let us rewrite (18) with explicit matrix indices as

$$\begin{aligned}\langle\Psi_0|\Psi_0\rangle = \langle 0 \,|\, & v_{L+1,\nu_{2L}} D_{L,\nu_{2L}\nu_{2L-1}} P_{L,\nu_{2L-1}\nu_{2L-2}} \cdots P_{2,\nu_3\nu_2} D_{1,\nu_2\nu_1} v_{1,\nu_1} \\ & \times v^\dagger_{1,\mu_1} D^\dagger_{1,\mu_1\mu_2} P^\dagger_{2,\mu_2\mu_3} \cdots P^\dagger_{L,\mu_{2L-2}\mu_{2L-1}} D^\dagger_{L,\mu_{2L-1}\mu_{2L}} v^\dagger_{L+1,\mu_{2L}}|0\rangle \ ,\end{aligned} \tag{19}$$

where summation over repeated indices is implied. The term $v_{1,\nu_1}v^{\dagger}_{1,\mu_1}$ is readily evaluated in the local vacuum $|0_1\rangle$, for there are no other terms involving site 1. It is then convenient to introduce a vector $|W\rangle = \langle 0_j|v_j \otimes v_j^{\dagger}|0_j\rangle$, i.e., $W_{\alpha_j} = \langle 0_j|v_{j,\nu_j}v^{\dagger}_{j,\mu_j}|0_j\rangle$ with $\alpha_j = (\nu_j\,,\mu_j)$. It is clear that the 16 entries of $|W\rangle$ are c numbers independent of site label. We may therefore commute $D^{\dagger}_{1,\mu_1\mu_2}$ through W_{α_1} and define a 16×16 c-number matrix $\mathcal{L}$ as the local-vacuum expectation value of the tensor (direct) product of D_i^T with $D_i^{\dagger}$, i.e., $\mathcal{L}_{\alpha\beta} = \langle 0_i|D^T_{i,\nu_{2i-1}\nu_{2i}}D^{\dagger}_{i,\mu_{2i-1}\mu_{2i}}|0_1\rangle$, where $\alpha = (\nu_{2i-1}\ ,\ \mu_{2i-1})$ and $\beta = (\nu_{2i}\ ,\ \mu_{2i})$. Next, we can commute $P_{2,\mu_2\mu_3}$ through $\mathcal{L}_{\alpha_1\alpha_2}$ and W_{α_1}, and define another 16×16 c-number matrix $\mathcal{M} = \langle 0_j|P_j^T \otimes P_j^{\dagger}|0_j\rangle$, and so forth. This procedure is continued until the last pair of supervectors in the product (19) is exhausted. The explicit forms of $|W\rangle, \mathcal{L}$, and $\mathcal{M}$ are given in Appendix B. The final expression is most compactly written by introducing another c-number vector $|Z\rangle = \mathcal{M}^{-1}|W\rangle$ as

$$\langle\Psi_0|\Psi_0\rangle = W_{\alpha_1}\mathcal{L}_{\alpha_1,\alpha_2}\mathcal{M}_{\alpha_2\alpha_3}\mathcal{L}_{\alpha_3\alpha_4}\cdots\ \mathcal{L}_{\alpha_{2L-1}\alpha_{2L}}\mathcal{M}_{\alpha_{2L}\alpha_{2L+1}}Z_{\alpha_{2L+1}}\ , \tag{20}$$

which leads to the simple result

$$\langle\Psi_0|\Psi_0\rangle = \langle W|\mathcal{T}^L|Z\rangle\ , \tag{21}$$

where $\mathcal{T} = \mathcal{L}\mathcal{M}$ is a c-number 16×16 matrix, the analog of the transfer matrix in statistical mechanics. The matrix $\mathcal{T}$ takes the explicit form (see Appendix B)

$$\mathcal{T} = \begin{bmatrix}
1+B & 0 & 0 & 0 & 0 & 0 & 0 & 0 & 0 & 0 & 1 & 0 & 0 & 0 & 0 & 1\\
0 & A & 0 & 0 & 0 & 0 & 0 & 0 & 0 & 0 & 0 & 0 & 0 & 0 & 0 & 0\\
0 & 0 & B & 0 & 0 & 0 & 0 & 0 & 0 & 0 & 0 & 0 & 0 & 1 & 0 & 0\\
0 & 0 & 0 & B & 0 & 0 & 0 & 0 & 0 & -1 & 0 & 0 & 0 & 0 & 0 & 0\\
0 & 0 & 0 & 0 & A & 0 & 0 & 0 & 0 & 0 & 0 & 0 & 0 & 0 & 0 & 0\\
A & 0 & 0 & 0 & 0 & A & 0 & 0 & 0 & 0 & A & 0 & 0 & 0 & 0 & A\\
0 & 0 & 0 & 0 & 0 & 0 & A & 0 & 0 & 0 & 0 & 0 & -A & 0 & 0 & 0\\
0 & 0 & 0 & 0 & 0 & 0 & 0 & A & A & 0 & 0 & 0 & 0 & 0 & 0 & 0\\
0 & 0 & 0 & 0 & 0 & 0 & 0 & 1 & B & 0 & 0 & 0 & 0 & 0 & 0 & 0\\
0 & 0 & 0 & -A & 0 & 0 & 0 & 0 & 0 & A & 0 & 0 & 0 & 0 & 0 & 0\\
B & 0 & 0 & 0 & 0 & 1 & 0 & 0 & 0 & 0 & B & 0 & 0 & 0 & 0 & 1\\
0 & 0 & 0 & 0 & 0 & 0 & 0 & 0 & 0 & 0 & 0 & A & 0 & 0 & 0 & 0\\
0 & 0 & 0 & 0 & 0 & 0 & -1 & 0 & 0 & 0 & 0 & 0 & B & 0 & 0 & 0\\
0 & 0 & A & 0 & 0 & 0 & 0 & 0 & 0 & 0 & 0 & 0 & 0 & A & 0 & 0\\
0 & 0 & 0 & 0 & 0 & 0 & 0 & 0 & 0 & 0 & 0 & 0 & 0 & 0 & A & 0\\
B & 0 & 0 & 0 & 0 & 1 & 0 & 0 & 0 & 0 & 1 & 0 & 0 & 0 & 0 & B
\end{bmatrix}\ , \tag{22}$$

where $A = \widetilde{V}^{-2}$ and $B = 1+\widetilde{V}^{-2}$. Unlike the usual case $\mathcal{T}$ is not symmetric. Moreover, the physical quantities of interest cannot be expressed in terms of the trace of the "transfer matrix" $\mathcal{T}$. Nevertheless, $\mathcal{T}$ has the useful property of being a normal matrix, i.e., $[\mathcal{T},\mathcal{T}^{\dagger}] = 0$. In other words, $\mathcal{T}$ can be diagonalized and so we have the spectral representation,

$$\mathcal{T} = \sum_{\alpha,a}\frac{\lambda_\alpha}{C_{\alpha a}}|R;\lambda_\alpha,a\rangle\langle L;\lambda_\alpha,a|\ , \tag{23}$$

where λ_α are the eigenvalues of $\mathcal{T}$ and $|R(L);\lambda_\alpha,a\rangle$ denote the corresponding right (left) eigenvectors with degeneracy label a. The eigenvalues and eigenvectors are obtained analytically with the help of Mathematica. For notational simplicity, we choose to work with unnormalized eigenvectors, i.e., $\langle L;\lambda_\alpha,a|R;\lambda_\beta,b\rangle = \delta_{\alpha\beta}\delta_{ab}C_{\alpha a}$ where $C_{\alpha,a}$ are the normalization constants (see Appendix B). The characteristic polynomial $P(\lambda)$ of $\mathcal{T}$ is found to be

$$P(\lambda) = (\lambda-A)^5(\lambda^2-[A+B]\lambda+A^2)^4 \times(\lambda^3-[1+3B]\lambda^2+[2+A(1+3B)]\lambda-A^3)\ . \tag{24}$$

From (24), we infer a fivefold degenerate eigenvalue $\lambda_1 = \widetilde{V}^{-2}$, two fourfold-degenerate eigenvalues $\lambda_2 = \frac{1}{2}+\widetilde{V}^{-2}-\frac{1}{2}\sqrt{1+4\widetilde{V}^{-2}}$ and $\lambda_3 = \frac{1}{2}+\widetilde{V}^{-2}+\frac{1}{2}\sqrt{1+4\widetilde{V}^{-2}}$, and three nondegenerate eigenvalues which are roots of the third-order polynomial on the right-hand side of (24). These can be written as

$$\lambda_4 = \frac{4}{3}+\widetilde{V}^{-2}+\frac{1}{3}\left(z^{\frac{1}{3}}+\overline{z}^{\frac{1}{3}}\right)\ , \tag{25}$$

$$\lambda_5 = \frac{4}{3}+\widetilde{V}^{-2}-\frac{1}{6}\left[\left(z^{\frac{1}{3}}+\overline{z}^{\frac{1}{3}}\right)-i\sqrt{3}\left(z^{\frac{1}{3}}-\overline{z}^{\frac{1}{3}}\right)\right]\ , \tag{26}$$

and

$$\lambda_6 = \frac{4}{3}+\widetilde{V}^{-2}-\frac{1}{6}\left[\left(z^{\frac{1}{3}}+\overline{z}^{\frac{1}{3}}\right)+i\sqrt{3}\left(z^{\frac{1}{3}}-\overline{z}^{\frac{1}{3}}\right)\right]\ , \tag{27}$$

where

$$z = 28+45\widetilde{V}^{-2}+i3^{\frac{3}{2}}\left[8+40\widetilde{V}^{-2}+85\widetilde{V}^{-4}+64\widetilde{V}^{-6}\right]^{\frac{1}{2}}.$$

In Fig. 2, we plot the different eigenvalues versus $\widetilde{V}^{-1}$. Note that all eigenvalues are real, positive, increase

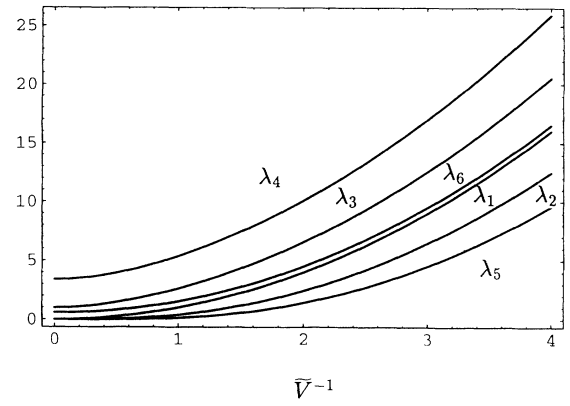

FIG. 2. The eigenvalues of the "transfer matrix" $\mathcal{T}$ versus $\widetilde{V}^{-1}$. Note that all eigenvalues are real, positive, increase monotonically with $\widetilde{V}^{-1}$, and do not cross.

monotonically with $\widetilde{V}^{-1}$ (as $\widetilde{V}^{-2}$ when $\widetilde{V}^{-1} \to \infty$) and do not cross. Equation (24) implies that at $\widetilde{V}^{-1} = 0$, $\lambda_1 = \lambda_2 = 0$, $\lambda_3 = 1$, $\lambda_4 = 2 + \sqrt{2}$, $\lambda_5 = 0$, and $\lambda_6 = 2 - \sqrt{2}$.

From the explicit form of the right (left) eigenvectors of $\mathcal{T}$, $|W\rangle$, and $|Z\rangle$, we infer the norm of the ground state as

$$\langle \Psi_0 | \Psi_0 \rangle = \sum_\alpha \frac{\lambda_\alpha^L}{C_{\alpha,1}} \rho_\alpha \,, \tag{28}$$

where the summation is over $\alpha = 4,5,6$ and $\rho_\alpha = \langle W|R;\lambda_\alpha,1\rangle\langle L;\lambda_\alpha,1|Z\rangle$. The eigenvalues λ_4,λ_5 and λ_6 contribute to the norm of the ground state whereas there is no contribution from the subspaces belonging to the eigenvalues λ_1, λ_2, and λ_3 because $\langle W|R;\lambda_\alpha,a\rangle = 0$ for $\alpha = 1,2,3$ (see Appendix B). The result (28) is exact for a finite chain of length L in units of the two-particle cell. From (2) it is clear that the norm (18) is a polynomial of degree $2L$ in $\widetilde{V}^{-1}$ while this is less obvious from (28).[10] Nevertheless, for the purpose of calculating physical quantities in the limit of an infinite system, Eq. (28) is appropriate. In the thermodynamic limit, the largest eigenvalue λ_4 dominates in (28), i.e.,

$$\langle \Psi_0 | \Psi_0 \rangle \approx \frac{\lambda_4^{L+1}\left(\lambda_4 + \widetilde{V}^{-2}\right)}{\left[3\left(\lambda_4 - \widetilde{V}^{-2}\right)^2 - 8\lambda_4 + 4\widetilde{V}^{-2} + 2\right]} \,, \tag{29}$$

where the fact that λ_4 is a root of the third-order polynomial in (24) has been used to simplify the final result.

We now pass to the evaluation of the expectation value of some local boson operator b_i. We discuss successively the charge density $b_i = n_i^\gamma$ and spin density $b_i = S_i^{z,\gamma}$, where $\gamma = d$ (p) for the Cu (O) site. The charge density, say, at a Cu site i, is given by

$$\langle n_i^d \rangle = \frac{\langle \Psi_0 | n_i^d | \Psi_0 \rangle}{\langle \Psi_0 | \Psi_0 \rangle} \,. \tag{30}$$

Using (16), the numerator on the right-hand side of (30) can be written as

$$\langle W^{(1)} | \mathcal{L}^{(1)} \mathcal{M}^{(2)} \ldots \mathcal{L}^{(i-1)} \mathcal{M}^{(i)} \mathcal{Q}_d^{(i)} \mathcal{M}^{(i+1)} \ldots \mathcal{L}^{(L)} \mathcal{M}^{(L+1)} | Z \rangle \,, \tag{31}$$

where $\mathcal{Q}_d^{(i)} = \langle 0_i | D_i^T \otimes n_i^d D_i^\dagger | 0_i \rangle$. For clarity, we have displayed upper indices in (31), though the c-number matrices are site independent. In this compact notation, we then have for $i \geq 1$

$$\langle n_i^d \rangle = \frac{\langle W | \mathcal{T}^{i-1} \mathcal{B}_d \mathcal{T}^{L-i} | Z \rangle}{\langle W | \mathcal{T}^L | Z \rangle} \,, \tag{32}$$

where $\mathcal{B}_d = \mathcal{Q}_d \mathcal{M}$. Similarly, the mean charge at an O site ($i \geq 2$) can be written as

$$\langle n_i^p \rangle = \frac{\langle W | \mathcal{T}^{i-2} \mathcal{B}_p \mathcal{T}^{L-i+1} | Z \rangle}{\langle W | \mathcal{T}^L | Z \rangle} \,, \tag{33}$$

where $\mathcal{B}_p = \mathcal{L}\mathcal{U}_p$, and $\mathcal{U}_p = \langle 0_j | P_j^T \otimes n_j^p P_j^\dagger | 0_j \rangle$. In the thermodynamic limit, the mean charge at a Cu site (O site) is parametrized by the eigenvalues λ_4, λ_5, and λ_6 as is seen on substitution of (23) into (32),

$$\langle n_i^d \rangle = \sum_\alpha \left(\frac{\lambda_\alpha}{\lambda_4}\right)^i \frac{\langle W|R;\lambda_\alpha,1\rangle\langle L;\lambda_\alpha,1|\mathcal{B}_d|R;\lambda_4,1\rangle\langle L;\lambda_4,1|Z\rangle}{C_\alpha \lambda_\alpha \rho_4} \tag{34}$$

respectively, into (33),

$$\langle n_i^p \rangle = \sum_\alpha \left(\frac{\lambda_\alpha}{\lambda_4}\right)^{i-1} \frac{\langle W|R;\lambda_\alpha,1\rangle\langle L;\lambda_\alpha,1|\mathcal{B}_p|R;\lambda_4,1\rangle\langle L;\lambda_4,1|Z\rangle}{C_\alpha \lambda_\alpha \rho_4} \tag{35}$$

where the summation is over $\alpha = 4,5,6$. The average charge at a Cu site (O site) in the bulk of the system reduces then to ($i \gg 1$)

$$\langle n_i^\gamma \rangle = \frac{\langle L;\lambda_4,1|\mathcal{B}_\gamma|R;\lambda_4,1\rangle}{C_4 \lambda_4} \,, \tag{36}$$

where (see Appendix B)

$$\langle L;\lambda_4,1|\mathcal{B}_d|R;\lambda_4,1\rangle = 2[a_4^L(1+a_4^R)+2+a_4^R+b_4^R]\,, \tag{37}$$

and

$$\langle L;\lambda_4,1|\mathcal{B}_p|R;\lambda_4,1\rangle = 2[a_4^L\left((1+A)a_4^R+2\right)+Ab_4^L(1+b_4^R)+Aa_4^R+2b_4^R+2(1+A)]\,. \tag{38}$$

In Fig. 3, we plot the bulk charge on the Cu site versus $\widetilde{V}^{-1}$. Substituing the explicit expressions for $\mathcal{B}_\gamma$, $\gamma = d\ (p)$, it can be verified that in the bulk of the chain there are two charges per unit cell as $\langle n_i^d\rangle + \langle n_i^p\rangle = 2$. In the Kondo regime ($\widetilde{V}^{-1} \ll 1$), there is on the average one electron at the Cu site and one at the O site while at small hybridization ($\widetilde{V}^{-1} \gg 1$) the Cu site empties in favor of a doubly occupied p site. In the latter limit, the strong on-site repulsion on the Cu sites becomes ineffective, and we expect the physics in this regime to be similar to that of the noninteracting system. In the thermodynamic limit, the largest eigenvalue λ_4 determines the local charge while λ_5 and λ_6 control the charge depletion on the Cu and O sites near the boundary of a long chain. For finite $\widetilde{V}$, the depletion region for charge has a width $\propto \left[\ln\left(\frac{\lambda_4}{\lambda_6}\right)\right]^{-1}$. Figure 4 illustrates the behavior of the charge near the boundary on the O sites. At large hybridization, the charge depletion takes place in a narrow region near the ends of the chain (for $\widetilde{V} \approx 100$, it is a few unit cells wide) while for small hybridization it extends over an extended region (for $\widetilde{V} \approx 0.1$, about 20–25 unit cells) away from the boundary. When $\widetilde{V}$ is large, the charge can accumulate on the Cu sites in the bulk and close to the boundary so that the Cu sites are nearly insensitive to the boundary effects (at $\widetilde{V} \approx 100$ the Cu charge drops within a few units cells by a relative amount of 10^{-5}!) whereas on the O sites the occupation drops to approximately half its value within a few unit cells. On the contrary, when the hybridization is small the boundary effects are substantial on the Cu sites because the occupation on the O sites should be close to two particles per site. This requires a considerable spread in the depletion width for both Cu and O sites.

Let us now calculate the average azimuthal spin $\langle S_i^{\gamma,z}\rangle = \langle\Psi_0|S_i^{\gamma,z}|\Psi_0\rangle/\langle\Psi_0|\Psi_0\rangle$ at an arbitrary site in the chain. Simple manipulations lead to the average spin, say, for a Cu site, as

$$\langle S_i^{d,z}\rangle = \frac{\langle W|\mathcal{T}^{i-1}\mathcal{S}_d^z\mathcal{T}^{L-i}|Z\rangle}{\langle W|\mathcal{T}^L|Z\rangle}\,. \tag{39}$$

Hence [see Eq. (23)],

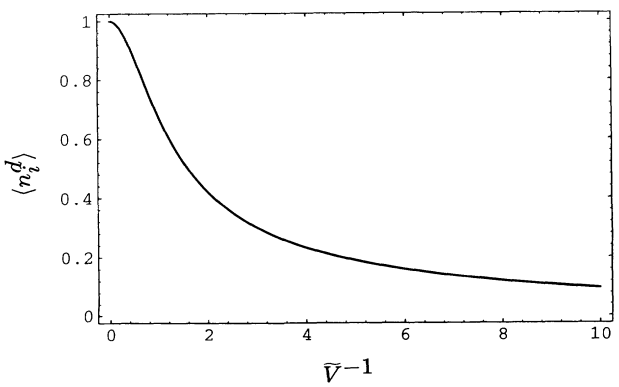

FIG. 3. Bulk charge on the d site versus $\widetilde{V}^{-1}$. In the Kondo limit ($\widetilde{V}^{-1} = 0$), the average occupation on the Cu site is 1. As the hybridization decreases to zero, the Cu site empties in favor of a doubly occupied O site.

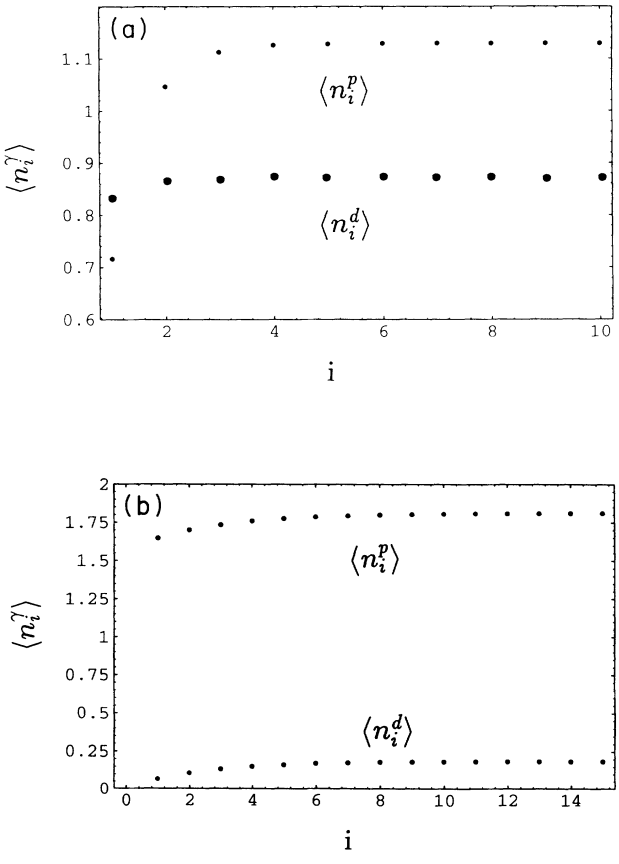

FIG. 4. (a) Boundary charge distribution on the O sites ($\langle n_i^p\rangle$) and Cu sites ($\langle n_i^d\rangle$) for $\widetilde{V}^{-1} = 5$. (b) Boundary charge distribution on the O sites ($\langle n_i^p\rangle$) and Cu sites ($\langle n_i^d\rangle$) for $\widetilde{V}^{-1} = 0.5$.

$$\langle S_i^{d,z}\rangle = \sum_\alpha \left(\frac{\lambda_\alpha}{\lambda_4}\right)^i \frac{\langle W|R;\lambda_\alpha,1\rangle\langle L;\lambda_\alpha,1|\mathcal{S}_d^z|R;\lambda_4,1\rangle\langle L;\lambda_4,1|Z\rangle}{C_\alpha\lambda_\alpha\rho_4}\ , \tag{40}$$

where $\mathcal{S}_d^z = \mathcal{Q}_d^z\mathcal{M}$ and $\mathcal{Q}_d^z = \langle 0_i|D_i^T\otimes S_i^{d,z}D_i^\dagger|0_j\rangle$. Using the explicit form of $\mathcal{S}_d^z$, it is straightforward to show that $\langle L;\lambda_\alpha,1|\mathcal{S}_d^z|R;\lambda_\beta,1\rangle = 0$ for $\alpha,\beta = 4,5,6$ while $\langle W|R;\lambda_\alpha,a\rangle = 0$ for $\alpha = 1,2,3$. In other words, the azimuthal spin at an arbitrary site vanishes in agreement with the singlet nature of the ground state. Notice that the expectation value of an arbitrary boson operator depends solely on the eigenvalues λ_α for $\alpha = 4,5,6$ and their corresponding right (left) eigenvectors because $\langle W|$ projects out the remaining subspaces. This is no longer true for the two-point correlation functions which we now consider.

The evaluation of equal-time two-point correlation functions for boson operators offers no new difficulty. Below we concentrate on the bulk correlations and neglect boundary effects. Up to a normalization factor, the charge-charge correlation function is given by $(i > j)$

$$\langle n_j^\gamma n_i^\gamma\rangle \propto \langle 0|v^{L+1}\ldots D_j n_j^\gamma P_j\ldots D_1 v_1\left[v_1^\dagger\right]^T D_1^\dagger\ldots D_{i-1}^\dagger P_i^\dagger n_i^\gamma D_i^\dagger P_{i+1}^\dagger\ldots D_L^\dagger v_{L+1}^\dagger|0\rangle\ , \tag{41}$$

for $\gamma = p,d$. In (41), we have commuted the boson operators $n_i^\gamma,\gamma = p,d$, through the local supermatrices so that their position is adjacent to the corresponding local matrices $D_i^{(\dagger)}$ $(P_i^{(\dagger)})$. We can then proceed as in the previous calculations, evaluate local expectation values, and in the thermodynamic limit we obtain $(\gamma = d,p)$

$$\langle n_j^\gamma n_i^\gamma\rangle - \langle n_j^\gamma\rangle\langle n_i^\gamma\rangle = \left(\frac{\lambda_6}{\lambda_4}\right)^{|i-j|}\frac{\langle L;\lambda_4,1|\mathcal{B}_\gamma|R;\lambda_6,1\rangle\langle L;\lambda_6,1|\mathcal{B}_\gamma|R;\lambda_4\rangle}{\lambda_4\lambda_6 C_4 C_6}\ , \tag{42}$$

where

$$\langle L;\lambda_4,1|\mathcal{B}_\gamma|R;\lambda_6,1\rangle = 2[2a_4^L + (1+A)a_4^L a_6^R + Ab_4^L(1+b_6^L) + Aa_6^R + 2b_6^R + 2(1+A)]\ , \tag{43}$$

and $\langle L;\lambda_6,1|\mathcal{B}_\gamma|R;\lambda_4,1\rangle$ follows from (43) by interchanging the indices $4,6\to 6,4$. The explicit form of the various terms in (43) is given in Appendix B. The charge-charge correlations are negative and decay exponentially on both Cu and O sites with identical correlation length $\xi_c = \left[\ln\left(\frac{\lambda_4}{\lambda_6}\right)\right]^{-1}$. This indicates that the system behaves as a single-component charged liquid. Note that ξ_c coincides with the decay length for charge depletion at the boundary and so only one length scale controls the charge degrees of freedom in the model {at $\widetilde{V}^{-1} = 0$, $\xi_c = \left[\ln\left(\frac{2+\sqrt{2}}{2-\sqrt{2}}\right)\right]^{-1}$ while as $\widetilde{V}^{-1}\to\infty$, $\xi_c \approx \frac{\widetilde{V}^{-1}}{2}$}. Figure 5 illustrates the nearest-neighbor charge correlations between the Cu sites and between the O sites as a function of $\widetilde{V}^{-1}$. In the Kondo limit, the charge fluctuations between Cu sites are completely suppressed as expected while the charge correlations between O sites are enhanced. The Cu-Cu correlations are naturally suppressed in the limit of small hybridization and therefore go through a maximum in absolute value at an intermediate value of $\widetilde{V}^{-1}\approx 1.6$.

The longitudinal spin-spin correlations for Cu and O sites are evaluated similarly as ($|i-j|\geq 1$ and $\gamma = d,p$)

$$\langle S_j^{z,\gamma}S_i^{z,\gamma}\rangle = \left(\frac{\lambda_1}{\lambda_4}\right)^{|i-j|}\frac{\langle L;\lambda_4,1|\mathcal{S}_\gamma^z|R;\lambda_1,1\rangle\langle L;\lambda_1,1|\mathcal{S}_\gamma^z|R;\lambda_4,1\rangle}{\lambda_4\lambda_1 C_{4,1}C_{1,1}}\ , \tag{44}$$

where $\mathcal{S}_p^z = \mathcal{L}\mathcal{U}_p^z$ with the definition $\mathcal{U}_p^z = \langle 0_j|P_j^T\otimes S_j^z D_j^\dagger|0_j\rangle$. Substituing the explicit form for the matrix elements, we arrive at

$$\langle S_j^{z,p}S_i^{z,p}\rangle = -\left(\frac{\lambda_1}{\lambda_4}\right)^{|i-j|}\frac{Aa_4^R\left(2+Ab_4^L\right)}{\lambda_4\lambda_1 C_{4,1}C_{1,1}}\ , \tag{45}$$

$$\langle S_j^{z,d}S_i^{z,d}\rangle = -\left(\frac{\lambda_1}{\lambda_4}\right)^{|i-j|}\frac{a_4^L\left(2+a_4^R+b_4^R\right)}{\lambda_4\lambda_1 C_{4,1}C_{1,1}}\ . \tag{46}$$

The spin-spin correlation function between Cu and O sites takes a different form, namely,

$$\langle S_j^{z,d}S_i^{z,p}\rangle = \left(\frac{\lambda_1}{\lambda_4}\right)^{|i-j|}\frac{\langle L;\lambda_4,1|\mathcal{S}_d^z|R;\lambda_1,1\rangle\langle L;\lambda_1,1|\mathcal{S}_p^z|R;\lambda_4,1\rangle}{\lambda_1^2 C_{4,1}C_{1,1}}\ , \tag{47}$$

which leads to

$$\langle S_j^{z,d}S_i^{z,p}\rangle = -\left(\frac{\lambda_1}{\lambda_4}\right)^{|i-j|}\frac{Aa_4^L a_4^R}{\lambda_1^2 C_{4,1}C_{1,1}}\ . \tag{48}$$

Note that the formula for the nearest-neighbor spin-spin correlation between Cu and O sites requires some modifications as the labeling of the sites refers to clusters. When $j = i\pm 1$, we have instead of (48) the following

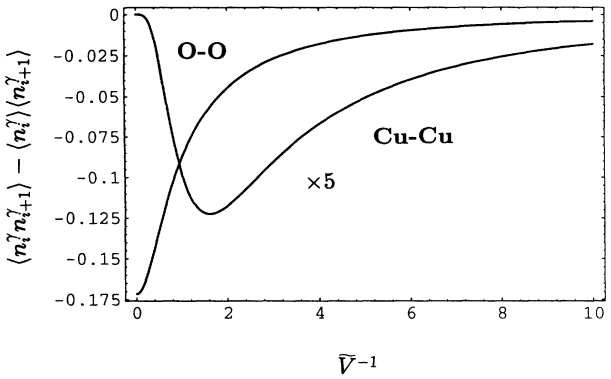

FIG. 5. Nearest-neighbor charge-charge correlation function for O sites (O-O) and for Cu sites (Cu-Cu). The Cu-Cu charge correlation function has been scaled by a factor of 5. As expected, the charge fluctuations are completely suppressed in the Kondo limit.

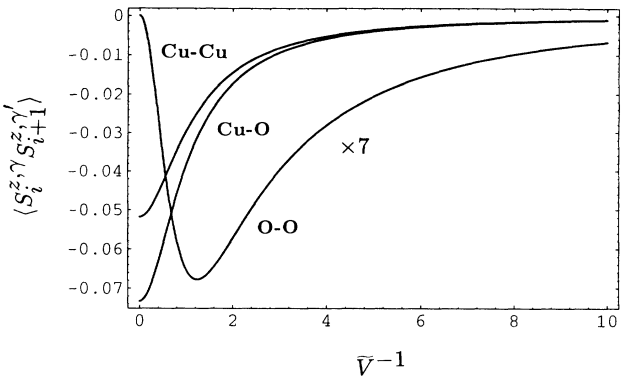

FIG. 6. Spin-spin correlation for nearest neighbors versus $\widetilde{V}^{-1}$ between Cu sites (Cu-Cu), between Cu and O sites (Cu-O) and between O sites (O-O). Notice that in the figure the O-O correlation function has been rescaled by a factor of 7. In the Kondo limit, the nearest-neighbor spin fluctuations between O sites vanish while between Cu sites and between Cu and O sites the probability for antiparallel alignment is substantial. This illustrates the inadequacy of a simple Néel picture with two antiparallel aligned sublattices.

result

$$\langle S_j^{z,d} S_i^{z,p} \rangle = \frac{\langle L;\lambda_4,1|\mathcal{G}^z|R;\lambda_4,1\rangle}{\lambda_4 C_{4,1}} = -\frac{a_4^R a_4^L}{2\lambda_4 C_{4,1}} \ , \qquad (49)$$

where $\mathcal{G}^z = \mathcal{Q}_d^z \mathcal{U}_p^z$. All spin-spin correlation functions are negative and decay exponentially with a correlation length $\xi_s = \left[\ln\left(\frac{\lambda_4}{\lambda_1}\right)\right]^{-1}$. In the whole range of parameters, ξ_s^{-1} is greater than ξ_c^{-1}. This however does not imply that the spin gap is greater than the charge gap since we have no information on the excitation spectrum.[12,13] Figure 6 illustrates the nearest-neigbor spin-spin correlations versus $\widetilde{V}^{-1}$. The decay lengths for both Cu and O holes are identical and this supports the physical picture of a single-component spin liquid involving the Cu and O sites. In the Kondo limit, the quantum fluctuations induce a 28% probablility of antiparallel alignment between the neighboring Cu and the O spins and a 20% probablility of antiparallel alignment between the neighboring Cu spins while the correlations between the O spins vanish. This is understood as a consequence of the fact that in this limit the wave function (2) is a superposition of pure local Zhang-Rice singlets.[3,11] Since all nearest-neighbor spin correlations are negative, the classical Néel picture does not apply to this class of insulators.

We next calculate the equal-time single-particle propagators for Cu and O holes, i.e.,

$$\langle f_{\gamma,j\sigma}^\dagger f_{\gamma,j\sigma} \rangle = \frac{\langle \Psi_0 | f_{\gamma,j\sigma}^\dagger f_{\gamma,j\sigma} | \Psi_0 \rangle}{\langle \Psi_0 | \Psi_0 \rangle} \ , \qquad (50)$$

where $f_{\gamma,j\sigma}^\dagger = d_{i\sigma}^\dagger$ for $\gamma = d$ and $f_{\gamma,j\sigma}^\dagger = p_{i\sigma}^\dagger$ for $\gamma = p$. First, consider the O-hole propagator and focus on the numerator of (50),

$$\langle p_{j\sigma}^\dagger p_{j\sigma} \rangle = \langle 0 | \left[v_{L+1}\right]^T D_L \ldots P_2 D_1 v_1 p_{j\sigma}^\dagger p_{j\sigma} \left[v_1^\dagger\right]^T D_1^\dagger P_2^\dagger \ldots D_L^\dagger v_{L+1}^\dagger | 0 \rangle \ . \qquad (51)$$

To evaluate (51), we need to commute fermion operators through a sequence of local $D^{(\dagger)}$ and $P^{(\dagger)}$ supermatrices. Each time a fermion operator is interchanged with a local matrix $D^{(\dagger)}$ ($P^{(\dagger)}$), the odd (fermionic) sector of the supermatrix picks up a minus sign. Introducing the notation $\widetilde{D}_i^\dagger$ and $\widetilde{P}_i^\dagger$, where

$$\widetilde{D}_i^\dagger = \begin{bmatrix} 0 & \widetilde{V}^{-1} & -d_{i,\downarrow}^\dagger & d_{i,\uparrow}^\dagger \\ \widetilde{V}^{-1} & 0 & 0 & 0 \\ -d_{i,\downarrow}^\dagger & 0 & 0 & -\widetilde{V}^{-1} \\ d_{i,\uparrow}^\dagger & 0 & \widetilde{V}^{-1} & 0 \end{bmatrix} , \qquad (52)$$

$$\widetilde{P}_j^\dagger = \begin{bmatrix} 1 & p_{j,\uparrow}^\dagger p_{j,\downarrow}^\dagger & -p_{j,\uparrow}^\dagger & -p_{j,\downarrow}^\dagger \\ p_{j,\uparrow}^\dagger p_{j,\downarrow}^\dagger & 0 & 0 & 0 \\ -p_{j,\uparrow}^\dagger & 0 & 0 & p_{j,\uparrow}^\dagger p_{j,\downarrow}^\dagger \\ -p_{j,\downarrow}^\dagger & 0 & -p_{j,\uparrow}^\dagger p_{j,\downarrow}^\dagger & 0 \end{bmatrix} , \qquad (53)$$

we commute the fermion operators so that (for $i > j$)

$$\langle p^\dagger_{j\sigma} p_{j\sigma}\rangle = \langle 0|\left[v_{L+1}\right]^T \ldots D_j P_j p^\dagger_{j\sigma} \widetilde{D}_{j-1} \ldots \widetilde{D}_1 \widetilde{v}_1 \left[\widetilde{v}^\dagger_1\right]^T \widetilde{D}^\dagger_1 \ldots \widetilde{P}^\dagger_j \widetilde{D}^\dagger_j \ldots \widetilde{D}^\dagger_{i-1} p_{i\sigma} P^\dagger_i \ldots D^\dagger_L v^\dagger_{L+1}|0\rangle \ , \tag{54}$$

where $\left[\widetilde{v}^\dagger_1\right]^T = \left[1, p^\dagger_{j\uparrow} p^\dagger_{j\downarrow}, -p^\dagger_{j\uparrow}, -p^\dagger_{j\downarrow}\right]$. From this point on, we proceed as in the evaluation of the correlation functions for boson operators and obtain

$$\langle p^\dagger_{j\sigma} p_{j\sigma}\rangle = \frac{\langle W|\mathcal{T}^{j-2}\mathcal{N}_{p,\sigma}\widetilde{\mathcal{T}}^{i-j-1}\mathcal{E}_{p,\sigma}\mathcal{T}^{L-i+1}|Z\rangle}{\langle W|\mathcal{T}^L|Z\rangle} \ , \tag{55}$$

where $\mathcal{N}_{p,\sigma} = \mathcal{L}\widetilde{\mathcal{U}}_{\sigma,p}$ and $\mathcal{E}_{p,\sigma} = \widetilde{\mathcal{L}}\mathcal{U}_{\sigma,p}$, with the definitions $\widetilde{\mathcal{U}}_{\sigma,p} = \langle 0_j|P^T_j \otimes p^\dagger_{j,\sigma}\widetilde{P}^\dagger_j|0_j\rangle$, $\mathcal{U}_{\sigma,p} = \langle 0_i|P^T_i \otimes p_{i,\sigma}P^\dagger_i|0_i\rangle$. In (55), we have used the notation $\widetilde{\mathcal{L}} = \langle 0_i|D^T_i \otimes \widetilde{D}^\dagger_i|0_i\rangle$, $\widetilde{\mathcal{M}} = \langle 0_j|P^T_j \otimes \widetilde{P}^\dagger_j|0_j\rangle$, and $\widetilde{\mathcal{T}} = \widetilde{\mathcal{L}}\widetilde{\mathcal{M}}$. The latter has the same eigenvalues and degeneracies as $\mathcal{T}$, yet its right (left) eigenvectors are different and labeled by $|\widetilde{R}\left(\widetilde{L}\right);\lambda_\alpha, a\rangle$ (see Appendix B). Similarly, the Cu-hole propagator follows as

$$\langle d^\dagger_{j\sigma} d_{j\sigma}\rangle = \frac{\langle W|\mathcal{T}^{j-1}\mathcal{N}_{d,\sigma}\widetilde{\mathcal{T}}^{i-j-1}\mathcal{E}_{d,\sigma}\mathcal{T}^{L-i}|Z\rangle}{\langle W|\mathcal{T}^L|Z\rangle} \ , \tag{56}$$

where $\mathcal{N}_{d,\sigma} = \widetilde{\mathcal{Q}}_{\sigma,d}\widetilde{\mathcal{M}}$, $\mathcal{E}_{d,\sigma} = \mathcal{Q}_{\sigma,d}\mathcal{M}$, and $\widetilde{\mathcal{Q}}_{\sigma,d} = \langle 0_j|D^T_j \otimes d^\dagger_{j,\sigma}\widetilde{D}^\dagger_j|0_j\rangle$, $\mathcal{Q}_{\sigma,d} = \langle 0_i|D^T_i \otimes d_{i,\sigma}D_i|0_i\rangle$. Using (23), the equal-time propagators become ($|i-j| \geq 1$),

$$\langle f^\dagger_{\gamma,j\sigma} f_{\gamma,i\sigma}\rangle = \left(\frac{\lambda_2}{\lambda_4}\right)^{|i-j|} \Omega^\gamma_{2,4} + \left(\frac{\lambda_3}{\lambda_4}\right)^{|i-j|} \Omega^\gamma_{3,4} \ , \tag{57}$$

for $\gamma = p, d$ and where

$$\Omega^\gamma_{\alpha,a} = \frac{\langle L;\lambda_4,1|\mathcal{N}_{\gamma,\sigma}|\widetilde{R};\lambda_\alpha,a\rangle\langle\widetilde{L};\lambda_\alpha,a|\mathcal{E}_{\gamma,\sigma}|R;\lambda_4,1\rangle}{\lambda_4\lambda_\alpha C_{4,1}C_{\alpha,4}} \ . \tag{58}$$

In (58) we have for $\alpha = 2,3$ (see Appendix B),

$$\langle L;\lambda_4,1|\mathcal{N}_{p,\sigma}|\widetilde{R};\lambda_\alpha,4\rangle = a^L_4 + Ab^L_4(1+a^{R,4}_\alpha) + 2a^{R,4}_\alpha + A + 2 \ , \tag{59}$$

$$\langle\widetilde{L};\lambda_\alpha,4|\mathcal{E}_{p,\sigma}|R;\lambda_4,1\rangle = -\left[1 + Aa^{L,4}_\alpha + a^R_4\left(Aa^{L,4}_\alpha + A + 1\right)\right] \ , \tag{60}$$

and

$$\langle L;\lambda_4,1|\mathcal{N}_{d,\sigma}|\widetilde{R};\lambda_\alpha,4\rangle = A\left[a^L_4 + a^{R,4}_\alpha + 1\right] \ , \tag{61}$$

$$\langle\widetilde{L};\lambda_\alpha,4|\mathcal{E}_{d,\sigma}|R;\lambda_4,1\rangle = -A\left[a^{L,4}_\alpha\left(a^R_4 + b^R_4 + 2\right) + a^R_4 + 1\right] \ . \tag{62}$$

The Cu- and O-hole propagators exhibit the characteristic exponential decay as do other correlation functions. This feature is a first indication that (2) does not describe a metallic state but rather an insulating state. While we have no information on the excitation spectrum, we can estimate the single-particle gap Δ using the relation $\xi_0^{-2} = \Delta/t$, where $\xi_0^{-1} = \ln\left(\frac{\lambda_4}{\lambda_3}\right)$ is the correlation length of the single-particle propagators [see (57)]. For $\widetilde{V} \ll 1$, we find $\Delta \approx \frac{V^2}{t}$, in agreement with the gap obtained in the noninteracting theory. It is tempting to use the same relation in the Kondo limit, in which case $\Delta \approx t\left[\ln\left(2+\sqrt{2}\right)\right]^2$. This is consistent with the interpretation that the model reduces to a Kondo lattice with $J \approx t$ discussed earlier.

For a finite chain with OBC, the system is not translationally invariant. In the thermodymamic limit, however, the Fourier transform of the equal-time propagator yields the exact momentum distribution for $\gamma = p, d$,

$$\langle n^\gamma_{k,\sigma}\rangle = \Omega^\gamma_{2,4}F(k;\xi_2) + \Omega^\gamma_{3,4}F(k;\xi_3) + \Omega^\gamma_0 \ , \tag{63}$$

where $\Omega^\gamma_0 = \frac{1}{2}\langle n^\gamma_i\rangle$, and

$$F(k;\xi_\alpha) = \frac{2e^{-\xi^{-1}_\alpha}\left[\cos(k) - e^{-\xi^{-1}_\alpha}\right]}{\left[1 + e^{-2\xi^{-1}_\alpha} - 2\cos(k)e^{-\xi^{-1}_\alpha}\right]} \ . \tag{64}$$

In Fig. 7, we plot the momentum distribution of O and Cu holes for different values of $\widetilde{V}$. The absence of singularity in $\langle n^\gamma_{k,\sigma}\rangle$ rules out a metallic state. In the Kondo limit, the momentum distribution for the Cu holes is completely flat. It becomes sharply peaked around $k = 0$ for small $\widetilde{V}$. In contrast, the momentum distribution for the O holes is peaked around $k = \pi$ in the Kondo limit, characteristic of a conduction band severely broadened by a large hybridization gap. For small $\widetilde{V}$, it is near

unity except for a narrow region around $k = 0$. We have compared these exact results for $\widetilde{V} \ll 1$ with the momentum distributions obtained in the free theory when $\widetilde{V}$ is small and found excellent agreement, except that in the free theory $\langle n_k^p \rangle = 0$ and $\langle n_k^d \rangle = 1$ at $k = 0$.

Similar manipulations to those presented above yield the ground-state amplitudes $\langle \phi_j \phi_i^\dagger \rangle$, where $\phi_i^\dagger = \sum_\sigma \sigma\, d_{i,\sigma}^\dagger \left(p_{i+1,-\sigma}^\dagger - p_{i,-\sigma}^\dagger \right)$, for the Zhang-Rice singlet,[11] $\phi_i^\dagger = p_{i,\uparrow}^\dagger p_{i\downarrow}^\dagger$ for O-O singlet, and $\phi_i^\dagger = d_{i,\uparrow}^\dagger d_{i+1,\downarrow}^\dagger$ for Cu-Cu singlet pairings. For example, for singlet pairing between neighboring Cu spins (O sites), a straightforward calculation leads to

$$\langle d_{j+1\downarrow} d_{j\uparrow} d_{i\uparrow}^\dagger d_{i+1\downarrow}^\dagger \rangle = \left(\frac{\lambda_1}{\lambda_4} \right)^{|i-j|} \frac{A^2 a_4^L \left(2a_4^R + b_4^R + 3 \right)}{\lambda_4^2 \lambda_1^2 C_{4,1} C_{1,5}} , \tag{65}$$

$$\langle p_{j\downarrow} p_{j\uparrow} p_{i\uparrow}^\dagger p_{i\downarrow}^\dagger \rangle = \left(\frac{\lambda_1}{\lambda_4} \right)^{|i-j|} \frac{A^2 a_4^R \left(A^2 b_4^R + 2 \right)}{\lambda_4^2 \lambda_1^2 C_{4,1} C_{1,4}} . \tag{66}$$

We find that all pairing amplitudes decay exponentially with the same characteristic inverse decay length $\xi_{\text{pairing}}^{-1} = \ln \left(\frac{\lambda_4}{\lambda_1} \right)$, which is identical to that of the longitudinal spin-spin correlation functions. This result implies the absence of off-diagonal long-range order (ODLRO) or power-law correlation for pairing in the singlet channel.

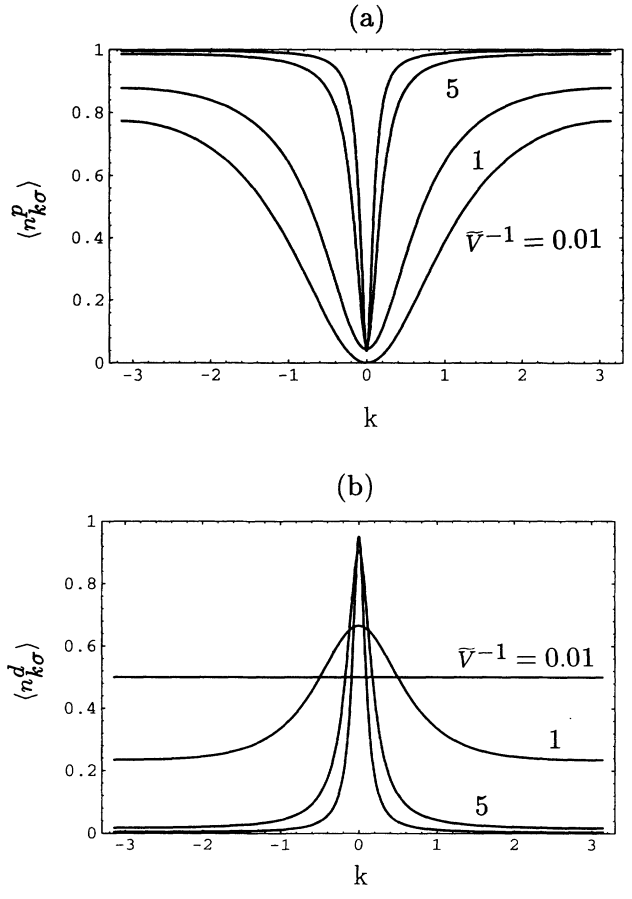

FIG. 7. Momentum distribution of (a) the O holes and (b) the Cu holes for $\widetilde{V}^{-1} = 0.01$, $\widetilde{V}^{-1} = 1$, $\widetilde{V}^{-1} = 5$, and $\widetilde{V}^{-1} = 10$. The absence of singularity in $\langle n_k^{d,p} \rangle$ rules out a metallic state. In the Kondo limit, the momentum distribution of the O holes is characteristic of a conduction band severely broadened by a large hybridization gap.

IV. GENERALIZATIONS

In this section we briefly discuss the doped Emery chain and various extensions of the model that have not been investigated in previous works.

A. Doped Emery chain

There are various ways to insert particles into the chain, the simplest one being $|\Psi_0^{(l)}\rangle = p_{l,\sigma}^\dagger |\Psi_0\rangle$, etc., as suggested by Brandt and Giesikus.[1] Let us write the ground state for a chain with an additional particle inserted, say, an up spin at the O site l,

$$\begin{aligned} |\Psi_{+1\uparrow}^l\rangle &= p_{l\uparrow}^\dagger |\Psi_0\rangle \\ &= \left[\tilde{v}_1^\dagger \right]^T \tilde{D}_1^\dagger \ldots \tilde{D}_{l-1}^\dagger p_{l\uparrow}^\dagger P_l^\dagger \ldots v_{L+1}^\dagger |0\rangle . \end{aligned} \tag{67}$$

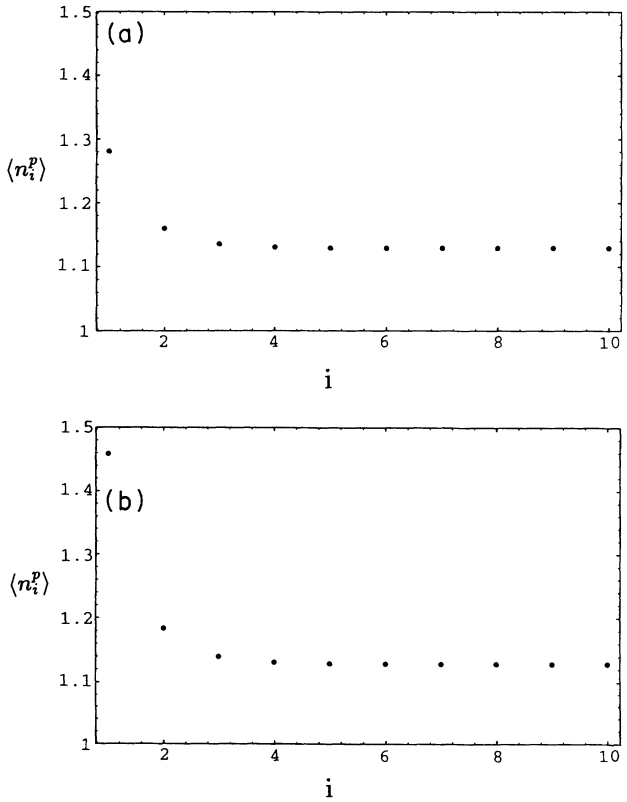

FIG. 8. Charge density on the O sites around the insertion site for $\widetilde{V}^{-1} = 0.5$ (a) in the bulk and (b) near the boundary. The additional charge is exponentially localized around the insertion site.

Applying techniques similar to those developped in the previous section and neglecting boundary effects ($l \gg 1$), we find

$$\frac{\langle \Psi^l_{+1\uparrow}|\Psi^l_{+1\uparrow}\rangle}{\langle \Psi_0|\Psi_0\rangle} = \frac{\langle L;\lambda_4,1|\mathcal{R}_{p\uparrow}|R;\lambda_4,1\rangle}{\lambda_4 C_{4,1}}\,, \tag{68}$$

where

$$\langle L;\lambda_4,1|\mathcal{R}_{p\uparrow}|R;\lambda_4,1\rangle = a_4^L a_4^R + Ab_4^L(1+a_4^R) + (2+A)a_4^R + 2\,. \tag{69}$$

From (68) it is easily seen that the norm is finite (see Appendix B). This result also holds true when inserting two particles and so forth. We may ask for the charge distribution around the insertion site ($i \neq l$) and this is readily shown to be ($|i-l|>1$)

$$\frac{\langle \Psi^l_{+1\uparrow}|n_i^p|\Psi^l_{+1\uparrow}\rangle}{\langle \Psi^l_{+1\uparrow}|\Psi^l_{+1\uparrow}\rangle} = \frac{\langle L;\lambda_4,1|\mathcal{B}_p|R;\lambda_4,1\rangle}{\lambda_4 C_{4,1}} + \left(\frac{\lambda_6}{\lambda_4}\right)^{|i-l|} \frac{\langle L;\lambda_4,1|\mathcal{R}_{p\uparrow}|R;\lambda_6,1\rangle\langle L;\lambda_6,1|\mathcal{B}_p|R;\lambda_4,1\rangle}{\lambda_6 C_{6,1}\langle L;\lambda_4,1|\mathcal{R}_{p\uparrow}|R;\lambda_4,1\rangle} + \left(\frac{\lambda_5}{\lambda_4}\right)^{|i-l|} \frac{\langle L;\lambda_4,1|\mathcal{R}_{p\uparrow}|R;\lambda_5,1\rangle\langle L;\lambda_5,1|\mathcal{B}_p|R;\lambda_4,1\rangle}{\lambda_5 C_{5,1}\langle L;\lambda_4,1|\mathcal{R}_{p\uparrow}|R;\lambda_4,1\rangle}\,, \tag{70}$$

where

$$\langle L;\lambda_4,1|\mathcal{R}_{p\uparrow}|R;\lambda_6,1\rangle = a_4^L a_6^R + Ab_4^L(1+a_6^R) + (2+A)a_6^R + 2\,, \tag{71}$$

and $\langle L;\lambda_4,1|\mathcal{R}_{p\uparrow}|R;\lambda_5,1\rangle$ is obained from (71) by the replacement $6 \to 5$. When $i = l$, (70) reduces to

$$\frac{\langle \Psi^l_{+1\uparrow}|n_l^p|\Psi^l_{+1\uparrow}\rangle}{\langle \Psi^l_{+1\uparrow}|\Psi^l_{+1\uparrow}\rangle} = \frac{\langle L;\lambda_4,1|\mathcal{O}_{p\uparrow}|R;\lambda_4,1\rangle}{\langle L;\lambda_4,1|\mathcal{R}_{p\uparrow}|R;\lambda_4,1\rangle}\,, \tag{72}$$

where

$$\langle L;\lambda_4,1|\mathcal{O}_{p\uparrow}|R;\lambda_4,1\rangle = 2a_4^L a_4^R + Ab_4^L(2+a_4^R) + 2(1+A)a_4^R + 4\,. \tag{73}$$

In Fig. 8 we plot the charge density measured from the doped site versus $\widetilde{V}^{-1}$. We find that the additional charge is exponentially localized around the insertion site. For large distances ($|i-l| \gg 1$), the decay length $\xi_{\text{doped}} \approx \left[\ln\left(\frac{\lambda_4}{\lambda_6}\right)\right]^{-1}$ coincides with the charge correlation length ξ_c of the undoped chain. At small hybridization, the charge is spread over a region of substantial width (at $\widetilde{V}^{-1} \approx 10$, it is about 15 unit cells) whereas at large hybridization it is localized within a few unit cells of the insertion site. This is consistent with the picture that at large hybridization the additional charge can easily be accommodated on the Cu and O sites. On the other hand, when $\widetilde{V}$ is small, the additional charge has to redistribute essentially among a large number of O and Cu sites. We have also investigated the charge distribution when the insertion site is at the boundary of a long chain. For comparison, we plot in Fig. 9 the charge density at the insertion site versus $\widetilde{V}^{-1}$. As expected, the charge accumulation on the insertion site is larger in the bulk than at the boundary. Note that we can also insert a (many) particle(s) in a state $p^\dagger_{k\sigma}$, with $k = \frac{\pi m}{L+2}$, $m = 1,\ldots,L+1$, and where $p^\dagger_{k,\sigma} = \sqrt{\frac{2}{L+2}}\sum_{j=1}^{L+1}\sin\left(\frac{\pi m}{L+2}j\right)p^\dagger_{j\sigma}$. The norm of this state is then related to the momentum distribution in an obvious way.

There exists an alternative way of doping the system which has not been noted previously. Consider the state

$$|\Psi_0^{2L+2}\rangle = \prod_{i=1,\sigma}^{l-1}\widetilde{\alpha}_i^\dagger\widetilde{\beta}_l^\dagger\prod_{i=l,\sigma}^{L}\widetilde{\alpha}_i^\dagger|0\rangle\,, \tag{74}$$

where $\widetilde{\alpha}_i^\dagger = \mathcal{P}\alpha^\dagger_{i,\uparrow}\alpha^\dagger_{i,\downarrow}\mathcal{P}$ and with the definition

$$\widetilde{\beta}_l^\dagger = p^\dagger_{l-a,\downarrow}d^\dagger_{l,\uparrow}p^\dagger_{l+a,\uparrow}p^\dagger_{l+a,\downarrow} - p^\dagger_{l-a,\uparrow}d^\dagger_{l,\downarrow}p^\dagger_{l+a,\uparrow}p^\dagger_{l+a,\downarrow} - p^\dagger_{l-a,\uparrow}p^\dagger_{l-a,\downarrow}d^\dagger_{l,\uparrow}p^\dagger_{l+a,\downarrow} + p^\dagger_{l-a,\uparrow}p^\dagger_{l-a,\downarrow}d^\dagger_{l,\downarrow}p^\dagger_{l+a,\uparrow}\,. \tag{75}$$

To show that (74) is an exact (highly degenerate) ground state of the doped system with two additional particles, it is sufficient to verify that

$$\widetilde{\alpha}^\dagger_{l\sigma}\widetilde{\beta}^\dagger_l = 0\,, \tag{76}$$

for $\sigma = \uparrow,\downarrow$, since $\left[\widetilde{\alpha}^\dagger_{j\sigma}\right]^2 = 0$ and $\{\widetilde{\alpha}^\dagger_{j\sigma},\widetilde{\beta}^\dagger_l\} = 0$ for $j \neq l$. In fact, we can increase the amount of doping by replacing an increasing number of β clusters at the cost of α

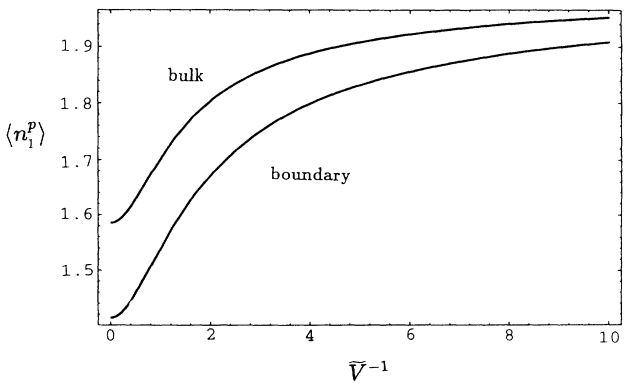

FIG. 9. Comparison bewteen the charge density at the insertion site (a) in the bulk and (b) at the boundary of a long chain. The charge excess at the insertion site is larger in the bulk than at the boundary as expected.

clusters until the chain is completely filled. (This corresponds to having half the clusters of α type and half of β type.) Defining a supermatrix $\Delta_l^\dagger$ as

$$\Delta_l^\dagger = \begin{bmatrix} 0 & 0 & 0 & 0 \\ 0 & 0 & d_{l,\downarrow}^\dagger & -d_{l,\uparrow}^\dagger \\ 0 & -d_{l,\downarrow}^\dagger & 0 & 0 \\ 0 & d_{l,\uparrow}^\dagger & 0 & 0 \end{bmatrix} , \tag{77}$$

we can simply write

$$\tilde{\beta}_l^\dagger = \left[v_l^\dagger\right]^T \Delta_l^\dagger v_l^\dagger . \tag{78}$$

Applying the techniques developed in the previous section, we can evaluate the charge distribution around the insertion sites. In all cases, we find that the charges are exponentially localized.[8] That the ground state of the doped chain is highly degenerate is a rather peculiar feature. Nonetheless, in the limit $\tilde{V} \to 0$, this massive degeneracy is consistent with the dispersionless upper hybridized band in the noninteracting system.

B. Chain with defects

We can solve the models of Refs. 1–4 with defects. The solvability condition leads to a set of constraints on the parameters of the model. For example, consider the 1D Emery model with one defect at lattice site l, i.e.,

$$\begin{aligned} H_{\mathcal{E}}^{\text{defect}} = H'_{\mathcal{E}} + \mathcal{P}[&t_0 \sum_\sigma \left(p_{l+1\sigma}^\dagger p_{l\sigma} + \text{H.c.}\right) \\ &+V_0 \sum_\sigma \left(d_{l\sigma}^\dagger \left(p_{l+1\sigma} - p_{l\sigma}\right) + \text{H.c.}\right) \\ &+\epsilon_d^0 \sum_\sigma \hat{n}_{l\sigma}^d + \epsilon_p^0 \sum_\sigma \left(\hat{n}_l^p + \hat{n}_{l+1}^p\right)]\mathcal{P} , \end{aligned} \tag{79}$$

where $H'_{\mathcal{E}}$ denotes the Hamiltonian (1) where the summation over j excludes the cluster l. Introducing the defect-cluster operators $\gamma_{l\sigma}^\dagger$ as

$$\gamma_{l\sigma}^\dagger = \frac{bV}{\sqrt{2t^2+V^2}} \left(d_{l\sigma}^\dagger - \frac{t_0}{V_0}\left[p_{l+1\sigma}^\dagger - p_{l\sigma}^\dagger\right]\right) , \tag{80}$$

the Hamiltonian (79) can be written as ($\tilde{d}_{l\sigma}^\dagger = \mathcal{P} d_{l\sigma}^\dagger \mathcal{P}$)

$$\begin{aligned} H_{\mathcal{E}}^{\text{defect}} = &\left[-N_\sigma C + 2\left(t - t_0\right) + \left(\epsilon_p + 2t\right)\hat{n}\right] L\mathcal{P} \\ &+C\left(\sum_{i(\neq l),\sigma} \tilde{\alpha}_{i\sigma}\tilde{\alpha}_{i\sigma}^\dagger + \sum_\sigma \tilde{\gamma}_{l\sigma}\tilde{\gamma}_{l\sigma}^\dagger\right) , \end{aligned} \tag{81}$$

provided that parameters are restricted to the manifold

$$b = \sqrt{\frac{t}{t_0}}\frac{V_0}{V_0} , \tag{82}$$

$$\epsilon_p + 2t = \epsilon_d + 2\frac{V^2}{t} , \tag{83}$$

$$V_0 = t_0\sqrt{\frac{\epsilon_p^0 - \epsilon_d^0 + t_0 + t}{2}} . \tag{84}$$

The Hamiltonian (81) comprises a constant and a positive semidefinite piece. The form (81) implies a unique ground state,

$$|\Psi_0^{\text{defect}}\rangle = \prod_{i=1,\sigma}^{l-1} \tilde{\alpha}_i^\dagger \tilde{\gamma}_l^\dagger \prod_{i=l,\sigma}^{L} \tilde{\alpha}_i^\dagger |0\rangle . \tag{85}$$

Again, dramatic simplifications occur in the calculations when introducing the supermatrix

$$I_l^\dagger = \begin{bmatrix} 0 & \sqrt{t_0 t} & \sqrt{\frac{t}{t_0}}V_0 d_{l,\downarrow}^\dagger & -\sqrt{\frac{t}{t_0}}V_0 d_{l,\uparrow}^\dagger \\ \sqrt{t_0 t} & 0 & 0 & 0 \\ \sqrt{\frac{t}{t_0}}V_0 d_{l,\downarrow}^\dagger & 0 & 0 & -\sqrt{t_0 t} \\ -\sqrt{\frac{t}{t_0}}V_0 d_{l,\uparrow}^\dagger & 0 & \sqrt{t_0 t} & 0 \end{bmatrix} , \tag{86}$$

and writting $\gamma_{l\uparrow}^\dagger \gamma_{l\downarrow}^\dagger$ as

$$\gamma_{l\uparrow}^\dagger \gamma_{l\downarrow}^\dagger = \left[v_l^\dagger\right]^T I_l^\dagger v_l^\dagger . \tag{87}$$

In this language, the evaluation of correlation functions is straightforward.[8]

C. 2D three-band model

Finally, we would like to point out that it is possible to solve a 2D three-band model where a copper atom is surrounded by four oxygen atoms in the plane. This model is physically closer to the original 2D Emery model than the d-p model discussed in Ref. 3. The Hamiltonian we consider is as follows

$$\begin{aligned} H_{\mathcal{E}}^{\text{2D}} = \mathcal{P}\Bigg[&\sum_{i,\sigma} \epsilon_d d_{i\sigma}^\dagger d_{i\sigma} + \sum_{i,\sigma} \epsilon_p p_{i\sigma}^\dagger p_{i\sigma} \\ &+t_{pd} \sum_{i,\sigma} \sum_{j\epsilon\{i\}} \left((-1)^{M_{ij}} d_{i\sigma}^\dagger p_{j\sigma} + \text{H.c.}\right) \\ &+t_{pp} \sum_{i,\sigma} \sum_{j\in\{i\}} \left((-1)^{N_{ij}} p_{i\sigma}^\dagger p_{j\sigma} + \text{H.c.}\right)\Bigg]\mathcal{P} , \end{aligned} \tag{88}$$

where

$$M_{ij} = \begin{cases} \text{even for } j = i - \frac{\hat{x}}{2} \text{ or } j = i - \frac{\hat{y}}{2} ; \\ \text{odd for } j = i + \frac{\hat{x}}{2} \text{ or } j = i + \frac{\hat{y}}{2} , \end{cases} \tag{89}$$

and

$$N_{ij} = \begin{cases} \text{even for } j = i + \frac{\hat{x}}{2} + \frac{\hat{y}}{2} ; \\ \text{odd for } j = i - \frac{\hat{x}}{2} - \frac{\hat{y}}{2} . \end{cases} \quad (90)$$

In the above formulas the Cu-Cu distance is taken as unit of distance, $\hat{x}$ and $\hat{y}$ denote a set of basis vectors, and $j \in \{i\}$ means that the sum is carried over nearest neighbors of the same ion type and so (88) contains a direct O-O hopping (through a central Cu site) which is absent in the original Emery model. The phases in (88) are chosen as in Ref. 11. We next define the cluster operators

$$\tilde{\alpha}^{\dagger}_{j\sigma} = \frac{1}{\sqrt{1+4t^2/V^2}} \mathcal{P} \Big[d^{\dagger}_{j\sigma} - \tilde{V}^{-1} \times \left(-p^{\dagger}_{j_1\sigma} - p^{\dagger}_{j_2\sigma} + p^{\dagger}_{j_3\sigma} + p^{\dagger}_{j_4\sigma} \right) \Big] \mathcal{P} , \quad (91)$$

where j_a, $a = 1,2,3,4$ label neighboring O sites starting from the right and moving counterclockwise around the central Cu ion. Moreover, we have set $t_{pd} = V$ and $t_{pp} = t$. The three-band Hamiltonian (88) can be separated into a constant and a positive semidefinite piece as

$$H^{2D}_{\mathcal{E}} = \left[-N_\sigma C' + (\epsilon_p + 2t)\, \hat{n} \right] L\mathcal{P} + C' \sum_{i,\sigma} \tilde{\alpha}_{i\sigma} \tilde{\alpha}^{\dagger}_{i\sigma} , \quad (92)$$

provided $\epsilon_d + 2\frac{V^2}{t} = \epsilon_p + 2t$ and where $C' = 4t + \frac{V^2}{t}$. Again, the form (92) allows us to show[8] that (88) has a unique ground state given by

$$|\Psi^{2D}_0\rangle = \prod_{j,\sigma} \tilde{\alpha}^{\dagger}_{i\sigma} |0\rangle . \quad (93)$$

It is interesting to note that for the Cu-O ceramics, $\epsilon_p - \epsilon_d \approx 3.6$ eV, a value that is consistent with the restriction $\epsilon_p - \epsilon_d = 2\left(\frac{V^2}{t} - t\right) \approx 3.9$ eV where $\frac{V}{t} = \frac{t_{pd}}{t_{pp}} \approx 2$ and $t_{pp} \approx 0.65$ eV (compare with Ref. 14). However, for a band filling corresponding to two particles per unit cell, the model (88) is far inside the highly doped regime and the solvability of (92) appears irrelevant to the interesting region of small doping. Though we have not succeeded in evaluating the correlation functions of the 2D three-band Emery model, we speculate that the ground state (93) describes an insulating state, which in the regime where $t_{pd} > t_{pp}$ should be of the Kondo type.

V. CONCLUSION

In summary, we have shown that the ground state of the 1D Emery model with infinite on-site repulsion on the copper sites is unique and evaluated all equal-time correlation functions in the ground state. We find that the latter decay exponentially with distance and that essentially three length scales (charge, spin, and propagator correlation lengths) determine the static properties of the model. While we have no information on the dynamics, our estimate of the single-particle gap is consistent with the result obtained in the small-hybridization limit. Our calculations suggest that the model interpolates between the intermediate-coupling Kondo lattice and the noninteracting band theory.

Moreover, it is worth emphasizing that the band filling for which the model is exactly solvable makes it inapplicable to the high-T_c superconductors. The exponentially decaying correlation functions as well as the fact that the insulating phase of the weak-hybridization limit is continuously connected to the Kondo regime imply that the ground state is an insulator for all values of the hybridization and does not exhibit ODLRO or power-law correlation in the singlet pairing channel. Based on the local structure of the wave function, we conjecture the absence of ODLRO in the singlet pairing channel for this class of wave functions in one and higher dimensions, in contrast with a recent speculation.[7]

We have doped the 1D Emery chain and found a massive degeneracy for the ground state of the doped system. This degeneracy, however, is a rather peculiar artifact which results from the restrictions in parameter space and forbids us to evaluate interesting properties.

We have shown that it is possible to introduce defects in the system without spoiling the solvability of the model and introduced a 2D three-band Emery model whose ground state is also solvable. Our exact results in 1D may be used to check approximations based on the slave fermion (boson) methods or as inspiration for new variational wave functions. The extensions of the method devised in this paper to other models such as the periodic Anderson model are straightforward, though numerical work is required in this case and a complete analytic solution is difficult.

ACKNOWLEDGMENTS

It is a pleasure to thank Y. Hatsugai and X.-G. Wen for stimulating discussions. We also wish to thank H. Tasaki for correspondence on the uniqueness of the ground state. This work is supported by NSF Grant No. DMR-92-16007.

APPENDIX A

This appendix is devoted to the proof of a lemma which we use in Sec. II.

Lemma

Consider a chain of $2L+1$ sites and let $|\Psi_0\rangle$ denote a state with $2L$ particles such that $\tilde{\alpha}^{\dagger}_{i,\sigma}|\Psi_0\rangle = 0$, for $i = 1,\ldots,L$ and $\sigma = \uparrow,\downarrow$. The cluster operators are defined by $\tilde{\alpha}^{\dagger}_{i,\sigma} = \sum_{\mu_i} a_{\mu_i} c^{\dagger}_{\mu_i,\sigma}$, where $c^{\dagger}_{\mu_i,\sigma}$ denotes a fermion or Hubbard operator with the property that $\left[c^{\dagger}_{\mu_i,\sigma}\right]^2 = 0$. Then $|\Psi_0\rangle$ can be written as

$$|\Psi_0\rangle = \sum_{\{\nu\}} \sum_{\{\nu'\}} A(\nu_1,\ldots,\nu_L|\nu'_1,\ldots,\nu'_L) c^\dagger_{\nu_1\uparrow}\cdots c^\dagger_{\nu_L\uparrow} c^\dagger_{\nu'_1\downarrow}\cdots c^\dagger_{\nu'_L\downarrow}|0\rangle \ , \tag{A1}$$

where $\{\nu\} = \{\nu_1 \le \nu_2 \le \ldots \nu_L\}$, and ν_j,ν'_j refer to lattice sites of the jth cluster (see Fig. 1). Note that the correlation of no double occupancy on the Cu sites is irrelevant to the lemma and the latter holds true even when the Hubbard operators are replaced by the usual fermion operators. Moreover, the generalization of this lemma to the models discussed in Refs. 1–4 in one and two dimensions is possible. For the 2D Emery model introduced in Sec. IV the proof is a straightforward extension of that presented below.

Proof

Without loss of generality, we restrict our discussion to the sector $S^z = 0$. Our first goal is to classify the three-site clusters according to the number of particles n_c and the value of azimuthal spin S^z_c which are not locally conserved quantities. We wish to verify in each case whether or not the corresponding cluster configuration fulfills a condition necessary (but not sufficient, see Sec. II) for the cluster to be annihilated by $\tilde{\alpha}^\dagger_{i,\sigma}$.

(1) $n_c = 0$ and $S^z_c = 0$ [see Fig. 10(a)]: Such a cluster cannot occur in a ground-state configuration. $\tilde{\alpha}^\dagger_{i,\sigma}$ is a linear combination of creation operators acting on different sites and so $\tilde{\alpha}^\dagger_{i,\sigma}|\text{cluster}\rangle = 0$ cannot be fulfilled locally for this cluster.

(2) $n_c = 1$ and $S^z_c = \pm\frac{1}{2}$ [see Fig. 10(b)]: This cluster cannot occur because $\tilde{\alpha}^\dagger_{i,\sigma}|\text{cluster}\rangle = 0$ cannot be fulfilled simultaneously for $\sigma =\uparrow$ and $\sigma =\downarrow$.

(3) $n_c = 2$ and $S^z_c = 0$ [see Fig. 10(c)]: This type of cluster is not inconsistent with the requirement that $\tilde{\alpha}^\dagger_{i,\sigma}|\text{cluster}\rangle = 0$, essentially because when acting on $|\Psi_0\rangle$ with $\tilde{\alpha}^\dagger_{i,\sigma}$ at least two identical configurations are generated which may cancel each other (provided the coefficients are appropriately chosen).

(4) $n_c = 2$ and $S^z_c = \pm 1$ [see Fig. 10(d)]: This type of cluster is not allowed because $\tilde{\alpha}^\dagger_{i,\sigma}|\text{cluster}\rangle = 0$ cannot be fulfilled simultaneously for $\sigma =\uparrow$ and $\sigma =\downarrow$.

(5) $n_c = 3$ and $S^z_c = \pm\frac{1}{2}$ [see Fig. 10(e)]: This type of cluster is not excluded *a priori* by the requirement that $\tilde{\alpha}^\dagger_{i,\sigma}|\text{cluster}\rangle = 0$.

(6) $n_c = 3$ and $S^z_c = \pm\frac{3}{2}$ [see Fig. 10(f)]: This type of cluster is not allowed as $\tilde{\alpha}^\dagger_{i,\sigma}|\text{cluster}\rangle = 0$ cannot be fulfilled simultaneously for $\sigma =\uparrow$ and $\sigma =\downarrow$.

(7) $n_c = 4$ and $S^z_c = 0$ [see Fig. 10(g)]: this type of cluster is allowed.

(8) $n_c = 4$ and $S^z_c = \pm 1$ [see Fig. 10(h)]: This type of cluster too is permitted.

(9) $n_c = 5$ and $S^z_c = \pm\frac{1}{2}$ [see Fig. 10(i)]: This type of cluster is not excluded by the requirement that $\tilde{\alpha}^\dagger_{i,\sigma}|\text{cluster}\rangle = 0$.

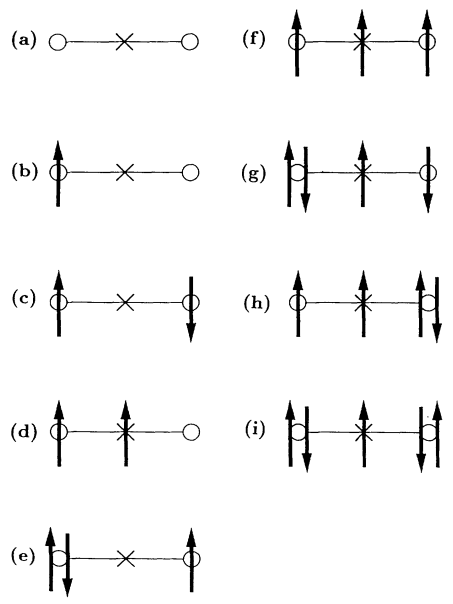

FIG. 10. Possible three-site clusters, with different numbers of particles and azimuthal spin, occurring in an arbitrary configuration.

Consider now an arbitrary configuration of $2L$ particles (L up spins) with no doubly occupied Cu sites. Classify, starting from the left end of the chain, all local cluster configurations in the above categories. If at least one cluster configuration encountered in this classification is of type (1), (2), (4), or (6), discard the corresponding configuration since $\tilde{\alpha}^\dagger_{i,\sigma}|\text{cluster}\rangle = 0$ cannot be fulfilled locally. We are then left with configurations which only contain clusters of types (3), (5), (7), (8), and (9).

For convenience, we now distinguish three cases:

(i) We first focus on configurations with no doubly occupied O sites. Since we have $2L$ particles for $2L + 1$ sites, there is one vacancy (unoccupied site). Therefore, there are $L - 1$ clusters of type (5) and one of type (3). Starting from the left end of the chain, we assign two-particle groups to each cluster as illustrated in Fig. 11. If, in this procedure, all two-particle groups drawn are of type (A) (see Fig. 11) the configuration under scrutinity can be written as

$$c^\dagger_{\nu_1\uparrow}\cdots c^\dagger_{\nu_L\uparrow} c^\dagger_{\nu'_1\downarrow}\cdots c^\dagger_{\nu'_L\downarrow}|0\rangle \ , \tag{A2}$$

where ν_j and ν'_j denote cluster indices as in (A1). Thus, the lemma is proven for this particular class of configurations.

Next, assume that we have a configuration $|c_1\rangle$ where at least one two-particle group of type (B) occurs [actually two of type (B) must occur simultaneously in a given configuration because $S^z_{\text{tot}} = 0$]. Denote by i_0 the position of the vacancy and by i_σ that of the type (B) group (see Fig. 11). The vacancy is surrounded by up and down spin since otherwise we would have a cluster of type (4) which is in contradiction with the above assumption. For $\tilde{\alpha}^\dagger_{i_0,\uparrow}|\Psi_0\rangle = 0$ to be fulfilled another configuration $|c_2\rangle$ should occur in $|\Psi_0\rangle$ where the vacancy is

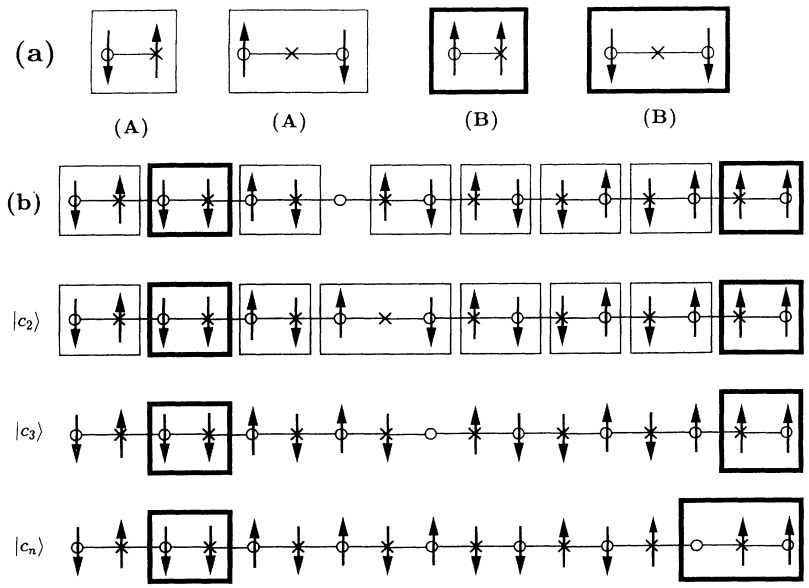

FIG. 11. Two-particle group assignment. (a) Various types of possible two-particle groups: (A) allowed and (B) forbidden. (b) Illustrative example of two-particle group assignment for a fixed configuration containing type (B) groups. We have also sketched some typical terms in the sequence of configurations $|c_1\rangle$, $|c_2\rangle$, etc., $|c_n\rangle$, where the latter contains a type (4) cluster.

located, say, to the right on a neighboring site (see Fig. 11). Of course, we could equally well choose another configuration $|c_2'\rangle$ for which the vacancy is located to the left of the original position. However, this freedom does not affect the argument given below. The new configuration $|c_2\rangle$ then should fulfill $\tilde{\alpha}^{\dagger}_{i,\downarrow}|\text{cluster}\rangle = 0$, which in turn requires another configuration $|c_3\rangle$, where the vacancy has now "moved" one further step to the right. The configuration $|c_3\rangle$ should as well fulfill $\tilde{\alpha}^{\dagger}_{i_0+1,\sigma}|\text{cluster}\rangle = 0$, and so forth. In this manner, the vacancy is succesively "propagated" to the right (left) and the set of equations (6) generates a (nonunique) sequence of configurations $|c_1\rangle,|c_2\rangle,|c_3\rangle,\ldots,|c_n\rangle$ (we assume that all members of the sequence label different configurations) so that the last configuration $|c_n\rangle$ has a vacancy adjacent to the group (B) (see Fig. 11). The latter contains a cluster of type (4) and that is inconsistent with the local constraint (6). Therefore the configuration $|c_n\rangle$ together with the whole sequence of ancestors should be discarded. Starting with $|c_1\rangle$, we may generate another sequence $|c_2'\rangle,|c_3'\rangle,\ldots$, yet after a finite number of steps we shall reach a configuration with a cluster of type (4), which similarly should be excluded in $|\Psi_0\rangle$. Had we focused on a configuration which contained groups of type (A) only, we would have generated sequences with no group of type (B). We conclude that for the type of configurations without doubly occupied O sites the lemma is proven.

(ii) Next consider configurations where clusters of type (3), (5), (7), and (8) occur. There are now N_D doubly occupied sites and so $N_v = N_d + 1$ vacancies. Starting from one end of the chain we assign two-particle groups to each three-site cluster sequentially until we reach the other end of the chain. If, in this process, no doubly occupied site occurs, we proceed as in (i). We may encounter a doubly occupied O site surrounded by an up and down spin so that there may be an apparent ambiguity in the group assignment (see Fig. 12). Since our aim is to factorize the configurations into cluster operators, we may choose the assigment such that the type (A) groups occur at the expense of the type (B) groups. Given a configuration with doubly occupied sites, we search for groups of the type (B) in each segment (delimited by vacancies). If a group of type (B) is adjacent to a doubly occupied site, we can generate a sequence of configurations using the constraint equations (6) which is such that the first term in the sequence has the doubly occupied site separated from the group of type (B) (see Fig. 12). The next configurations in the sequence will involve a vacancy "moving" successively to the type (B) group and at the end of the procedure a cluster of type (4) will emerge. According to the above arguments, the associated sequence of configurations should be excluded from the state $|\Psi_0\rangle$. In this manner we have eliminated all configurations which cannot be written as in (A2). Ergo, the lemma is proven for this case.

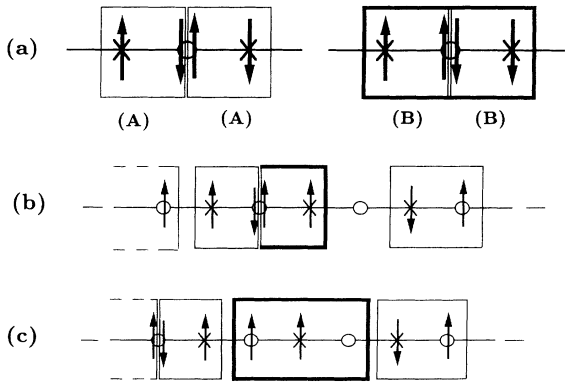

FIG. 12. (a) Possible two-particle assignment when doubly occupied sites appear: The prescription we adopt is to choose (1) whenever (2) occurs. (b) Illustrative example for a configuration with doubly occupied sites and its associated two-particle assignment. (c) Last term in the sequence where the doubly occupied sites have been separated from the type (B) group and a cluster of type (4) has emerged.

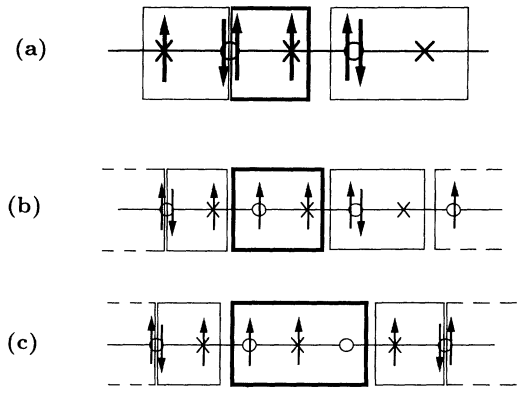

FIG. 13. (a) Environment for a cluster of type (9). (b) The type (9) cluster: separating the type (B) group from the doubly occupied sites. (c) The final term in the sequence with a cluster of type (4).

(iii) Consider finally configurations which include clusters of type (3), (5), (7), (8), and (9). Again, starting from one end of the chain we shall form all two-particle groups. If a cluster of type (9) occurs, then at least one adjacent cluster must have a vacancy on the Cu site (see Fig. 13). Otherwise, the excess accumulation of particles in the cluster of type (9) implies the presence of another cluster of type (2) which is forbidden. If a group of type (B) coincides with the type (9) cluster, we first build a sequence of configurations (this is always possible) such that the doubly occupied site becomes separated from the group of type (B). Then, by proceeding as in (i), we generate a sequence that contains at least one cluster of type (4) and so the whole sequence should be discarded.

Thus we are left with configurations that consist only of type (A) groups. This completes the proof that the state $|\Psi_0\rangle$ can be expanded as in (7).

APPENDIX B

In this Appendix, we present explicit expressions for the matrices $\mathcal{L}$,$\mathcal{M}$, etc. and the right (left) eigenvectors of $\mathcal{T}$ which are referred to in the bulk of the paper.

The vector $|W\rangle = \langle 0_j|v_j \otimes v_j^\dagger|0_j\rangle$, which projects into the subspace generated by λ_4, λ_5, and λ_6, is given by

$$|R;\lambda_1,1\rangle = [1\ 0\ 0\ 0\ 0\ 1\ 0\ 0\ 0\ 0\ 1\ 0\ 0\ 0\ 0\ 1\ ], \tag{B1}$$

while $|Z\rangle = \mathcal{M}^{-1}|W\rangle$ is simply

$$|Z\rangle = [1\ 0\ 0\ 0\ 0\ 0\ 0\ 0\ 0\ 0\ 0\ 0\ 0\ 0\ 0\ 0\ ], \tag{B2}$$

as is readily seen by inspecting the first column of $\mathcal{M}$ (see below). The matrices $\mathcal{L} = \langle 0_i|D_i^T \otimes D_i^\dagger|0_i\rangle$ and $\mathcal{M} = \langle 0_i|P_i^T \otimes P_i^\dagger|0_i\rangle$ are given respectively by

$$\mathcal{L} = \begin{bmatrix}
0 & 0 & 0 & 0 & 0 & A & 0 & 0 & 0 & 0 & 1 & 0 & 0 & 0 & 0 & 1 \\
0 & 0 & 0 & 0 & A & 0 & 0 & 0 & 0 & 0 & 0 & 0 & 0 & 0 & 0 & 0 \\
0 & 0 & 0 & 0 & 0 & 0 & 0 & -A & 1 & 0 & 0 & 0 & 0 & 0 & 0 & 0 \\
0 & 0 & 0 & 0 & 0 & 0 & A & 0 & 0 & 0 & 0 & 0 & 1 & 0 & 0 & 0 \\
0 & A & 0 & 0 & 0 & 0 & 0 & 0 & 0 & 0 & 0 & 0 & 0 & 0 & 0 & 0 \\
A & 0 & 0 & 0 & 0 & 0 & 0 & 0 & 0 & 0 & 0 & 0 & 0 & 0 & 0 & 0 \\
0 & 0 & 0 & -A & 0 & 0 & 0 & 0 & 0 & 0 & 0 & 0 & 0 & 0 & 0 & 0 \\
0 & 0 & A & 0 & 0 & 0 & 0 & 0 & 0 & 0 & 0 & 0 & 0 & 0 & 0 & 0 \\
0 & 0 & 1 & 0 & 0 & 0 & 0 & 0 & 0 & 0 & 0 & 0 & 0 & -A & 0 & 0 \\
0 & 0 & 0 & 0 & 0 & 0 & 0 & 0 & 0 & 0 & 0 & 0 & -A & 0 & 0 & 0 \\
-1 & 0 & 0 & 0 & 0 & 0 & 0 & 0 & 0 & 0 & 0 & 0 & 0 & 0 & 0 & A \\
0 & 0 & 0 & 0 & 0 & 0 & 0 & 0 & 0 & 0 & 0 & 0 & 0 & 0 & -A & 0 \\
0 & 0 & 0 & 1 & 0 & 0 & 0 & 0 & 0 & A & 0 & 0 & 0 & 0 & 0 & 0 \\
0 & 0 & 0 & 0 & 0 & 0 & 0 & 0 & A & 0 & 0 & 0 & 0 & 0 & 0 & 0 \\
0 & 0 & 0 & 0 & 0 & 0 & 0 & 0 & 0 & 0 & 0 & -A & 0 & 0 & 0 & 0 \\
1 & 0 & 0 & 0 & 0 & 0 & 0 & 0 & 0 & 0 & A & 0 & 0 & 0 & 0 & 0
\end{bmatrix}, \tag{B3}$$

$$\mathcal{M} = \begin{bmatrix}
1 & 0 & 0 & 0 & 0 & 1 & 0 & 0 & 0 & 0 & 1 & 0 & 0 & 0 & 0 & 1 \\
0 & 0 & 0 & 0 & 0 & 0 & 0 & 1 & 0 & 0 & 0 & 0 & 0 & 0 & 0 & 0 \\
0 & 0 & 0 & 0 & 0 & 0 & 0 & 1 & 1 & 0 & 0 & 0 & 0 & 0 & 0 & 0 \\
0 & 0 & 0 & 0 & 0 & 0 & -1 & 0 & 0 & 0 & 0 & 0 & 1 & 0 & 0 & 0 \\
0 & 1 & 0 & 0 & 1 & 0 & 0 & 0 & 0 & 0 & 0 & 0 & 0 & 0 & 0 & 0 \\
1 & 0 & 0 & 0 & 0 & 0 & 0 & 0 & 0 & 0 & A & 0 & 0 & 0 & 0 & 0 \\
0 & 0 & 0 & 1 & 0 & 0 & 0 & 0 & 0 & 0 & 0 & 0 & 0 & 0 & 0 & 0 \\
0 & 0 & -1 & 0 & 0 & 0 & 0 & 0 & 0 & 0 & 0 & 0 & 0 & 0 & 0 & 0 \\
0 & 0 & 1 & 0 & 0 & 0 & 0 & 0 & 0 & 0 & 0 & 0 & 0 & 1 & 0 & 0 \\
0 & 0 & 0 & 0 & 0 & 0 & 0 & 0 & 0 & 0 & 0 & 0 & 1 & 0 & 0 & 0 \\
1 & 0 & 0 & 0 & 0 & 0 & 0 & 0 & 0 & 0 & 0 & 0 & 0 & 0 & 0 & 1 \\
0 & 0 & 0 & 0 & 0 & 0 & 0 & 0 & 0 & 0 & 0 & 0 & 0 & 0 & -1 & 0 \\
0 & 0 & 0 & 1 & 0 & 0 & 0 & 0 & 0 & -1 & 0 & 0 & 0 & 0 & 0 & 0 \\
0 & 0 & 0 & 0 & 0 & 0 & 0 & 0 & -1 & 0 & 0 & 0 & 0 & 0 & 0 & 0 \\
0 & 0 & 0 & 0 & 0 & 0 & 0 & 0 & 0 & 0 & 0 & -1 & 0 & 0 & 0 & 0 \\
1 & 0 & 0 & 0 & 0 & 0 & 0 & 0 & 0 & 0 & 1 & 0 & 0 & 0 & 0 & 0
\end{bmatrix}. \tag{B4}$$

We now list all (right and left) eigenvectors of the "transfer matrix" $\mathcal{T}$. The λ_1 right eigensubspace is five dimensional and is spanned by

$$|R;\lambda_1,1\rangle = [0\ 0\ 0\ 0\ 0\ 0\ 0\ 0\ 0\ 0\ -1\ 0\ 0\ 0\ 0\ 1\ ]\,, \tag{B5}$$

$$|R;\lambda_1,2\rangle = [0\ 0\ 0\ 0\ 0\ 0\ 0\ 0\ 0\ 0\ 0\ 0\ 0\ 0\ 1\ 0\ ]\,, \tag{B6}$$

$$|R;\lambda_1,3\rangle = [0\ 0\ 0\ 0\ 0\ 0\ 0\ 0\ 0\ 0\ 0\ 1\ 0\ 0\ 0\ 0\ ]\,, \tag{B7}$$

$$|R;\lambda_1,4\rangle = [0\ 0\ 0\ 0\ 1\ 0\ 0\ 0\ 0\ 0\ 0\ 0\ 0\ 0\ 0\ 0\ ]\,, \tag{B8}$$

$$|R;\lambda_1,5\rangle = [0\ 1\ 0\ 0\ 0\ 0\ 0\ 0\ 0\ 0\ 0\ 0\ 0\ 0\ 0\ 0\ ]\,. \tag{B9}$$

The right eigensubspace to λ_2 is spanned by

$$|R;\lambda_2,1\rangle = \left[0\ 0\ a_2^{R,1}\ 0\ 0\ 0\ 0\ 0\ 0\ 0\ 0\ 0\ 1\ 0\ 0\ \right]\,, \tag{B10}$$

$$|R;\lambda_2,2\rangle = \left[0\ 0\ 0\ 0\ 0\ 0\ a_2^{R,2}\ 0\ 0\ 0\ 0\ 0\ 1\ 0\ 0\ 0\ \right]\,, \tag{B11}$$

$$|R;\lambda_2,3\rangle = \left[0\ 0\ 0\ a_2^{R,3}\ 0\ 0\ 0\ 0\ 0\ 1\ 0\ 0\ 0\ 0\ 0\ 0\ \right]\,, \tag{B12}$$

$$|R;\lambda_2,4\rangle = \left[0\ 0\ 0\ 0\ 0\ 0\ 0\ a_2^{R,4}\ 1\ 0\ 0\ 0\ 0\ 0\ 0\ 0\ \right]\,, \tag{B13}$$

where $a_2^{R,1} = \frac{\lambda_2 - A}{A}$, $a_2^{R,2} = -\frac{A}{\lambda_2 - A}$, $a_2^{R,3} = -a_2^{R,1}$ and $a_2^{R,4} = -a_2^{R,2}$. The right eigensubspace to λ_3 is spanned by

$$|R;\lambda_3,1\rangle = \left[0\ 0\ a_3^{R,1}\ 0\ 0\ 0\ 0\ 0\ 0\ 0\ 0\ 0\ 1\ 0\ 0\ \right]\,, \tag{B14}$$

$$|R;\lambda_3,2\rangle = \left[0\ 0\ 0\ 0\ 0\ 0\ a_3^{R,2}\ 0\ 0\ 0\ 0\ 0\ 1\ 0\ 0\ 0\ \right]\,, \tag{B15}$$

$$|R;\lambda_3,3\rangle = \left[0\ 0\ 0\ a_3^{R,3}\ 0\ 0\ 0\ 0\ 0\ 1\ 0\ 0\ 0\ 0\ 0\ 0\ \right]\,, \tag{B16}$$

$$|R;\lambda_4,4\rangle = \left[0\ 0\ 0\ 0\ 0\ 0\ 0\ a_4^{R,4}\ 1\ 0\ 0\ 0\ 0\ 0\ 0\ 0\ \right]\,, \tag{B17}$$

where $a_3^{R,1} = \frac{\lambda_3 - A}{A}$, $a_3^{R,2} = -\frac{A}{\lambda_3 - A}$, $a_3^{R,3} = -a_3^{R,1}$, and $a_3^{R,4} = -a_3^{R,2}$. The right eigenvectors to the nondegenerate eigenvalues λ_4, λ_5 and λ_6 are, respectively,

$$|R;\lambda_4,1\rangle = [a_4^R\ 0\ 0\ 0\ 0\ b_4^R\ 0\ 0\ 0\ 0\ 1\ 0\ 0\ 0\ 0\ 1\ ]\,, \tag{B18}$$

$$|R;\lambda_5,1\rangle = [a_5^R\ 0\ 0\ 0\ 0\ b_5^R\ 0\ 0\ 0\ 0\ 1\ 0\ 0\ 0\ 0\ 1\ ]\,, \tag{B19}$$

$$|R;\lambda_6,1\rangle = [a_6^R\ 0\ 0\ 0\ 0\ b_6^R\ 0\ 0\ 0\ 0\ 1\ 0\ 0\ 0\ 0\ 1\ ]\,, \tag{B20}$$

where $a_j^R = \frac{2}{\lambda_j - A - 2}$ and $b_j^R = \lambda_j - A - 2 - \frac{2(1+A)}{\lambda_j - A - 2}$ for $j = 4,5,6$.

The left and right eigenvectors to λ_1 are identical. The left eigensubspaces to λ_j with $j = 2,3$ are obtained by performing the replacement $a_j^{R,a} \to a_j^{L,a}$ in (B10)–(B17) where $a_j^{L,1} = \lambda_j - A$, $a_j^{L,2} = -\frac{1}{\lambda_j - A}$, $a_j^{L,3} = -a_j^{L,1}$ and $a_j^{L,4} = -a_j^{L,2}$. Finally, the left eigenvectors to λ_j with $j = 4,5,6$ are as in (B18)–(B20) except for the replacement $a_j^{R,a} \to a_j^{L,a}$ and $b_j^{R,a} \to b_j^{L,a}$, where $a_j^L = \lambda_j - A - 2 - \frac{2A}{\lambda - A}$ and $b_j^L = \frac{2}{\lambda - A}$.

The normalization constants follow then as $C_{\alpha,a} = \delta_{\alpha\beta}\delta_{ab}\langle L;\lambda_\alpha,a|R;\lambda_\beta,b\rangle$: $C_{1,1} = 2$ and $C_{1,a} = 1$ for $a = 2,3,4,5$; $C_{\alpha,a} = 1 + a_\alpha^{R,b}a_\alpha^{L,a}$ for $\alpha = 2,3$ and $a = 1,2,3,4$; $C_{\alpha,1} = 2 + a_\alpha^R a_\alpha^L + b_\alpha^R b_\alpha^L$ for $\alpha = 4,5,6$. Moreover, the weights $\rho_\alpha = \langle W|R;\lambda_\alpha,1\rangle\langle L;\lambda_\alpha,1|Z\rangle$ are readily calculated as $\rho_\alpha = a_\alpha^L\left(a_\alpha^R + b_\alpha^R + 2\right)$, for $\alpha = 4,5,6$.

It would excessively lengthen the paper, should we display all matrices $\mathcal{Q}_\gamma$, $\mathcal{B}_p$, $\mathcal{S}_d^z$, etc. Since the method of performing a direct product and evaluating expectation values is elementary, we shall omit most of these matrices and content ourselves with mentioning the matrices $\widetilde{\mathcal{L}}$, $\widetilde{\mathcal{M}}$, and $\widetilde{\mathcal{T}}$ which are required in the evaluation of the fermion propagators. The latter differ from $\mathcal{L}$, $\mathcal{M}$, and $\mathcal{T}$ by important phases which take into account the fermion nature of the underlying particles. Below, we also give the right (left) eigenvectors of $\widetilde{\mathcal{T}}$. Notice first that $\mathcal{L} = \langle 0_i|\widetilde{D}_i^T \otimes \widetilde{D}_i^\dagger|0_i\rangle$, $\mathcal{M} = \langle 0_i|\widetilde{P}_i^T \otimes \widetilde{P}_i^\dagger|0_i\rangle$, and $|W\rangle = \langle 0_j|\widetilde{v}_j \otimes \widetilde{v}_j^\dagger|0_j\rangle$. On the other hand, $\widetilde{\mathcal{L}} = \langle 0_i|D_i^T \otimes \widetilde{D}_i^\dagger|0_i\rangle$ and $\widetilde{\mathcal{M}} = \langle 0_i|P_i^T \otimes \widetilde{P}_i^\dagger|0_i\rangle$ are given by

$$\widetilde{\mathcal{L}} = \begin{bmatrix}
0 & 0 & 0 & 0 & 0 & A & 0 & 0 & 0 & 0 & -1 & 0 & 0 & 0 & 0 & -1 \\
0 & 0 & 0 & 0 & A & 0 & 0 & 0 & 0 & 0 & 0 & 0 & 0 & 0 & 0 & 0 \\
0 & 0 & 0 & 0 & 0 & 0 & 0 & -A & -1 & 0 & 0 & 0 & 0 & 0 & 0 & 0 \\
0 & 0 & 0 & 0 & 0 & 0 & A & 0 & 0 & 0 & 0 & 0 & -1 & 0 & 0 & 0 \\
0 & A & 0 & 0 & 0 & 0 & 0 & 0 & 0 & 0 & 0 & 0 & 0 & 0 & 0 & 0 \\
A & 0 & 0 & 0 & 0 & 0 & 0 & 0 & 0 & 0 & 0 & 0 & 0 & 0 & 0 & 0 \\
0 & 0 & 0 & -A & 0 & 0 & 0 & 0 & 0 & 0 & 0 & 0 & 0 & 0 & 0 & 0 \\
0 & 0 & A & 0 & 0 & 0 & 0 & 0 & 0 & 0 & 0 & 0 & 0 & 0 & 0 & 0 \\
0 & 0 & -1 & 0 & 0 & 0 & 0 & 0 & 0 & 0 & 0 & 0 & 0 & -A & 0 & 0 \\
0 & 0 & 0 & 0 & 0 & 0 & 0 & 0 & 0 & 0 & 0 & 0 & -A & 0 & 0 & 0 \\
1 & 0 & 0 & 0 & 0 & 0 & 0 & 0 & 0 & 0 & 0 & 0 & 0 & 0 & 0 & A \\
0 & 0 & 0 & 0 & 0 & 0 & 0 & 0 & 0 & 0 & 0 & 0 & 0 & 0 & -A & 0 \\
0 & 0 & 0 & -1 & 0 & 0 & 0 & 0 & 0 & A & 0 & 0 & 0 & 0 & 0 & 0 \\
0 & 0 & 0 & 0 & 0 & 0 & 0 & 0 & A & 0 & 0 & 0 & 0 & 0 & 0 & 0 \\
0 & 0 & 0 & 0 & 0 & 0 & 0 & 0 & 0 & 0 & 0 & -A & 0 & 0 & 0 & 0 \\
-1 & 0 & 0 & 0 & 0 & 0 & 0 & 0 & 0 & 0 & A & 0 & 0 & 0 & 0 & 0
\end{bmatrix}, \tag{B21}$$

$$\widetilde{\mathcal{M}} = \begin{bmatrix}
1 & 0 & 0 & 0 & 0 & 1 & 0 & 0 & 0 & 0 & -1 & 0 & 0 & 0 & 0 & -1 \\
0 & 0 & 0 & 0 & 0 & 0 & 0 & 1 & 0 & 0 & 0 & 0 & 0 & 0 & 0 & 0 \\
0 & 0 & 0 & 0 & 0 & 0 & 0 & 1 & -1 & 0 & 0 & 0 & 0 & 0 & 0 & 0 \\
0 & 0 & 0 & 0 & 0 & 0 & -1 & 0 & 0 & 0 & 0 & 0 & -1 & 0 & 0 & 0 \\
0 & 1 & 0 & 0 & 0 & 0 & 0 & 0 & 0 & 0 & 0 & 0 & 0 & 0 & 0 & 0 \\
1 & 0 & 0 & 0 & 0 & 0 & 0 & 0 & 0 & 0 & A & 0 & 0 & 0 & 0 & 0 \\
0 & 0 & 0 & 1 & 0 & 0 & 0 & 0 & 0 & 0 & 0 & 0 & 0 & 0 & 0 & 0 \\
0 & 0 & -1 & 0 & 0 & 0 & 0 & 0 & 0 & 0 & 0 & 0 & 0 & 0 & 0 & 0 \\
0 & 0 & -1 & 0 & 0 & 0 & 0 & 0 & 0 & 0 & 0 & 0 & 1 & 0 & 0 & 0 \\
0 & 0 & 0 & 0 & 0 & 0 & 0 & 0 & 0 & 0 & 0 & 0 & 1 & 0 & 0 & 0 \\
-1 & 0 & 0 & 0 & 0 & 0 & 0 & 0 & 0 & 0 & 0 & 0 & 0 & 0 & 0 & 1 \\
0 & 0 & 0 & 0 & 0 & 0 & 0 & 0 & 0 & 0 & 0 & 0 & 0 & 0 & -1 & 0 \\
0 & 0 & 0 & -1 & 0 & 0 & 0 & 0 & 0 & -1 & 0 & 0 & 0 & 0 & 0 & 0 \\
0 & 0 & 0 & 0 & 0 & 0 & 0 & 0 & -1 & 0 & 0 & 0 & 0 & 0 & 0 & 0 \\
0 & 0 & 0 & 0 & 0 & 0 & 0 & 0 & 0 & 0 & 0 & -1 & 0 & 0 & 0 & 0 \\
-1 & 0 & 0 & 0 & 0 & 0 & 0 & 0 & 0 & 0 & 1 & 0 & 0 & 0 & 0 & 0
\end{bmatrix}, \tag{B22}$$

and $\widetilde{\mathcal{T}} = \widetilde{\mathcal{L}}\widetilde{\mathcal{M}}$,

$$\widetilde{\mathcal{T}} = \begin{bmatrix}
1+B & 0 & 0 & 0 & 0 & 0 & 0 & 0 & 0 & 0 & -1 & 0 & 0 & 0 & 0 & -1 \\
0 & A & 0 & 0 & 0 & 0 & 0 & 0 & 0 & 0 & 0 & 0 & 0 & 0 & 0 & 0 \\
0 & 0 & B & 0 & 0 & 0 & 0 & 0 & 0 & 0 & 0 & 0 & 0 & -1 & 0 & 0 \\
0 & 0 & 0 & B & 0 & 0 & 0 & 0 & 0 & 1 & 0 & 0 & 0 & 0 & 0 & 0 \\
0 & 0 & 0 & 0 & A & 0 & 0 & 0 & 0 & 0 & 0 & 0 & 0 & 0 & 0 & 0 \\
A & 0 & 0 & 0 & 0 & A & 0 & 0 & 0 & 0 & -A & 0 & 0 & 0 & 0 & -A \\
0 & 0 & 0 & 0 & 0 & 0 & A & 0 & 0 & 0 & 0 & 0 & A & 0 & 0 & 0 \\
0 & 0 & 0 & 0 & 0 & 0 & 0 & A & -A & 0 & 0 & 0 & 0 & 0 & 0 & 0 \\
0 & 0 & 0 & 0 & 0 & 0 & 0 & -1 & B & 0 & 0 & 0 & 0 & 0 & 0 & 0 \\
0 & 0 & 0 & A & 0 & 0 & 0 & 0 & 0 & A & 0 & 0 & 0 & 0 & 0 & 0 \\
-B & 0 & 0 & 0 & 0 & -1 & 0 & 0 & 0 & 0 & B & 0 & 0 & 0 & 0 & 1 \\
0 & 0 & 0 & 0 & 0 & 0 & 0 & 0 & 0 & 0 & 0 & A & 0 & 0 & 0 & 0 \\
0 & 0 & 0 & 0 & 0 & 0 & 1 & 0 & 0 & 0 & 0 & 0 & B & 0 & 0 & 0 \\
0 & 0 & -A & 0 & 0 & 0 & 0 & 0 & 0 & 0 & 0 & 0 & 0 & A & 0 & 0 \\
0 & 0 & 0 & 0 & 0 & 0 & 0 & 0 & 0 & 0 & 0 & 0 & 0 & 0 & A & 0 \\
-B & 0 & 0 & 0 & 0 & -1 & 0 & 0 & 0 & 0 & 1 & 0 & 0 & 0 & 0 & B
\end{bmatrix}. \tag{B23}$$

The characteristic polynomial of $\widetilde{\mathcal{T}}$ is identical to that of $\mathcal{T}$ [see Eq. (24)] and so the eigenvalues of the two matrices coincide. The right (left) eigensubspaces to λ_1 for both matrices are identical. On the other hand, the right (left) eigenvectors to λ_α for $\alpha = 2, 3$ are obtained from (B10)–(B17) by the replacement $a_\alpha^{R,a} \to \widetilde{a}^{R,a}$, where $\widetilde{a}^{R,a} = -a_\alpha^{R,a}$ for $a = 1, 2, 3, 4$ ($a_\alpha^{L,a} \to \widetilde{a}^{L,a}$, where $\widetilde{a}^{L,a} = -a_\alpha^{L,a}$). Similarly, the right (left) eigenvectors to λ_α, $\alpha = 4, 5, 6$ follow from the substitution $a_\alpha^R \to \widetilde{a}^a$, where $\widetilde{a}^R = -a_\alpha^R$ ($a_\alpha^L \to \widetilde{a}^L$, where $\widetilde{a}^L = -a_\alpha^L$).

---

*Present address: Institut Laue-Langevin, Ave des Martyrs, B.P. 156, 38042 Grenoble, Cedex 9, France.

[1]U. Brandt and A. Giesekus, Phys. Rev. Lett. **68**, 2648 (1992).

[2]A. Mielke, J. Phys. A **25**, 6507 (1992).

[3]R. Strack, Phys. Rev. Lett. **70**, 833 (1993).

[4]R. Strack and D. Vollhardt (unpublished).

[5]More precisely, the number of particles per unit cell is equal to the degeneracy of the underlying fermions. For fermions of spin s with no orbital degeneracy the number of particles per unit cell is $2s + 1$, etc.

[6]I. Affleck, T. Kennedy, E. H. Lieb, and H. Tasaki, Commun. Math. Phys. **115**, 477 (1988); W. D. Freitag and E. Müller-Hartmann, Z. Phys. B **83**, 381 (1991); A. Klümper, A. Schadschneider, and J. Zittartz, *ibid.* **87**, 281 (1992).

[7]H. Tasaki, Phys. Rev. Lett. **70**, 3303 (1992).

[8]P.-A. Bares and P. A. Lee (unpublished).

[9]Very recently, Tasaki has managed to prove the uniqueness of the ground state by induction on the number of unit cells [H. Tasaki (private communication)]. Our proof of the uniqueness of the ground state is based on a different argument.

[10]For a finite system, one can show directly that the norm (2) is a polynomial of degree $2L$ in $\widetilde{V}^{-1}$ where the coefficient of $\widetilde{V}^{-2L}$ is $(L+1)^2$ and the constant term is a solution to the the recursion relation $r_L = 4r_{L-1} - 2r_{L-2}$ with $r_1 = 4$ and $r_2 = 14$.

[11]F. C. Zhang and T. M. Rice, Phys. Rev. B **37**, 3759 (1988).

[12]Z. Wang, X.-P. Li, and D.-H. Lee, Phys. Rev. B **47**, 11 935 (1993).

[13]C. C. Yu and S. White (unpublished).

[14]M. Schlüter, M. S. Hybertsen, and M. Christensen, Phys. Rev. B **39**, 9028 (1989).